# Mechanics of Column Beds: II. Modeling of Coupled Stress-Strain-Flow Behavior

**Bee Gaik Yew and Jorge Ureta**
Dept. of Civil and Environmental Engineering, The University of Tennessee, Knoxville, TN, 37996 and
Div. of Chemical and Analytical Sciences, Oak Ridge National Laboratory, Oak Ridge, TN 37831

**R. Andrew Shalliker**
Center for Biostructural and Biomolecular Research, University of Western Sydney,
Richmond, NSW, 1797 Australia

**Eric C. Drumm**
Dept. of Civil and Environmental Engineering, The University of Tennessee, Knoxville, TN 37996

**Georges Guiochon**
Div. of Chemical and Analytical Sciences, Oak Ridge National Laboratory, Oak Ridge, TN and
Dept. of Chemistry, The University of Tennessee, Knoxville, TN, 37996

*The rheological behavior of a bed of packing material during its consolidation was investigated using an elastic-plastic model, the Frictional Material Model. This model takes into account the behavior of the packing material under compression stress, its consolidation, its internal friction, its friction against the column wall, and the dependence of the bed's permeability on the local void fraction. The complexity of the problem arises from the nonlinear behavior of the relationships between the critical parameters controlling the column bed behavior and the external stresses applied to this bed. Solutions of the model were calculated for combinations of axial compression and seepage stresses, the latter corresponding to the flow of the mobile-phase stream under typical conditions used in HPLC. The results demonstrate the importance of the internal angle of friction of the packing material used on the degree of radial and axial heterogeneity of the beds of chromatographic columns packed with this material.*

## Introduction

In Part I of this article (Yew et al., 2003), we reported on the results of the determination, for two different common packing materials, Zorbax C18 and Kromasil C8, of several parameters that are important for any investigation of the rheology of the beds of chromatographic columns. The parameters investigated were: (1) the swelling and the compression indices of the bed during its consolidation; (2) the coefficient of friction between the two packing materials and the stainless steel wall of the column; and (3) the permeability of beds consolidated under different degrees of stress. Together, the swelling and the compression indices of the bed characterize its behavior during consolidation under mechanical stress, that is, they permit the calculation of the variation of the local void fraction of the bed with the stress applied during the first consolidation step and during latter steps. The ratio of the coefficient of interfacial friction and the coefficient of internal friction of very similar materials previously reported agree well with the conventional Potyondy (1961) correlation. The permeabilities obtained are consistent with those calculated from the void ratio, using the Kozeny-Carman equation (Carman, 1956; Bird et al., 1960; Lambe and Whitman, 1979), although the dependence on the void ratio in the narrow interval within which determinations were possible seems somewhat different from the one predicted by the equation. These experimental data are required for the modeling of the rheology of the beds of columns used in

Correspondence concerning this article should be addressed to G. Guiochon.
Current address of B. G. Yew: GZA GeoEnvironmental Inc., One Edgewater Drive, Norwood, MA 02062.

preparative chromatography. In this work, we study the response of a slurry of packing material to an axial compression of the bed in the so-called "axial compression columns" and the effects of the coupling of mechanical and seepage effects during the preparation of chromatographic columns.

Over the past 30 years, a considerable amount of interest has been devoted to the development of suitable procedures to prepare chromatographic columns by filling an appropriate tube with a convenient packing material for liquid chromatography. Because the particles of the materials used are very small (approximately between 2 and 20 $\mu$m), they can be dry-packed only with great difficulties and moderate success (Huber et al., 1972; Verzele and Dewaele, 1986). This method is now abandoned (Snyder and Kirkland, 1979; Poole and Poole, 1993). Two basic slurry procedures are currently in use, a slurry filtration and a slurry compression procedure. In both methods, a slurry of the packing material in a solvent that disperses well the packing particles is first prepared. In slurry filtration (Verzele and Dewaele, 1986: Snyder and Kirkland, 1979; Poole and Poole, 1993), this slurry is pumped into a tube of appropriate size, closed at the opposite end by a frit. The requisite volume of slurry is pushed by a clear solvent. A bed of particles accumulate behind the frit. The flow rate during the process is high; the pressure reached at the end of the operation exceeds 50 MPa and sometimes is as high as 70 MPa. The whole process is fast, usually taking no longer than a few minutes. Obviously, this procedure has many variables. Their influence has been studied only empirically (Verzele and Dewaele, 1986; Snyder and Kirkland, 1979; Poole and Poole, 1993). Most of these investigations focused on the nature of the slurry solvent and the good dispersion of the packing particles in this solvent. Limited attention was paid to the slurry density and to its flow rate, and almost none was paid to the critical operation of removal of the excess solvent from the slurry to pack the bed.

In slurry compression (Guiochon et al., 1997), the column is closed at one end by a piston, placed in a low position. The proper amount of slurry is poured into the column, which is then closed with a flange, and the piston is moved upward. Both the piston and the flange contain a flow distributor and a porous frit in contact with the bed. The excess solvent leaks out through these frits and a bed is formed, consolidated under the compression stress applied through the piston, which is actuated with a jack (Godbille and Tondu, 1976; Godbille and Devaux, 1976; Guiochon et al., 1996). The performance (column efficiency, porosity, and permeability) of the beds obtained by slurry filtration and by slurry compression are usually comparable over a wide range of column diameters (ca. 1 to 800 mm). The separation power of the column prepared seem to depend more on the skills and care of the operator than on which variant of either method was used. Comparable results were also obtained using other mechanical compression methods (such as radial) (Guiochon et al., 1997).

Until most recently, no satisfactory explanation was given to the origins of the radial heterogeneity of the beds obtained by any variant of these two consolidation methods (Farkas et al., 1997; Guiochon et al., 1997). Yet, this heterogeneity explains why the efficiency of a whole column is barely half of its potential efficiency, as suggested by measures of the local apparent dispersion coefficient of the column bed (Guiochon et al., 1997; Tallarek et al., 1996) and by a comparison of the best performance of conventional columns and of columns packed with particles having a diameter larger than one-tenth of the column diameter (Guiochon et al., 1997). This heterogeneity is explained by a wall effect (Knox et al., 1976), most probably arising from the consequences of the intense friction of the bed against the column wall (Guiochon et al., 1999; Cherrak and Guiochon, 2001). Yet, in spite of the importance of increasing the column efficiency to improve the production rate in preparative chromatography (or to reduce analysis times), there had been so far only one study applying the rheology of particulate materials to the investigation of the packing of chromatographic columns (Yuan et al., 1998). While this study provided some important insights into the mechanics of column packing, its results were limited by some of the modeling assumptions. It assumed that there is no slip at the wall, but that the friction of the bed against the wall is infinite. It used the von Mises yield criterion that is more suitable for metals than for beds of separate, rigid particles such as silica which exhibit a demonstrated frictional component of strength (Mihlbachler et al., 1998). It did not attempt to predict the radial heterogeneity of the compressed bed eventually obtained.

The objective of this work is to improve our understanding of the consolidation process that takes place between the moment when the particles in the slurry come into contact with their neighbors, ceasing to be nearly independent of each other, and the moment when these particles become frozen into a rigid organization in which they have practically no freedom of movement.

## Theory

As often in engineering, the solution of a problem such as the one studied here requires first the idealization of the actual physical problem into a mathematical model, then the construction of an algorithm for the computation of numerical solutions of this model. Because of the nature of the problem, a finite-element solution of the model was preferred to alternative approaches.

### *Physical model of the column consolidation process*

Conventionally, a column is prepared by filling a large steel tube, closed by a fine frit at one end, with a slurry of the packing material in a suitable solvent (see Figure 1). A piston is then pushed at a controlled velocity into the tube. It separates the packing material, which cannot filter through the frit, from the solvent, which flows through the frit and is collected in an external tank. Applying a proper mechanical stress to the piston compresses the slurry into a dense bed of the packing material. (NB. Although the compression piston also ends in a proper flow distributor and could be used to drain the slurry solvent, columns are always packed by draining the solvent from the end opposite this piston.) The consolidation of the bed into an HPLC column is achieved within a few seconds to a few minutes, depending on decisions made by the operator during the procedure. The consolidation of the bed is progressive, however, beginning at the end of the column opposite to the piston, which is the end through which the packing solvent flows out of the column, leaving the pack-

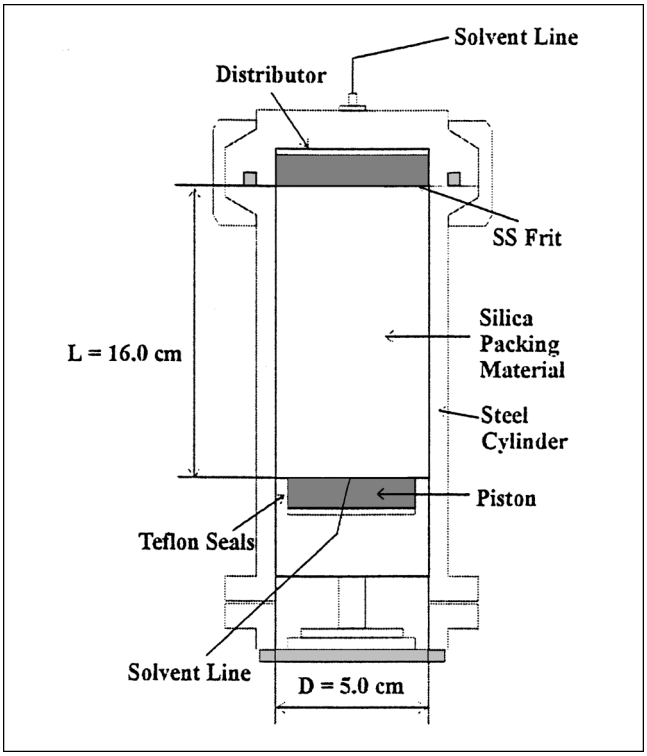


**Figure 1. Axial compression column for preparative HPLC.**

Dimensions are for the LC 50 "axial compression column skid" (Novasep, NJ) used in laboratory experiments (Farkas et al., 1997; Guiochon et al., 1999; Sarker et al., 1996).

ing material behind. Thus, the preparation of a column combines constraints of both mechanical and seepage origins.

We will not consider here the behavior of the slurry during the first part of the bed preparation, when the excess solvent is removed from the slurry. As long as the particles are not in contact, any displacement of the piston results in the expulsion of the corresponding volume of slurry solvent, but there is no mechanical resistance of the slurry to this movement. The external porosity of a slurry remains markedly higher than that of a bed, even when poorly consolidated. Hence, the permeability of the column is much higher when it is filled with a slurry, even a dense one, than when the particles are in contact. The rate at which the excess solvent is eliminated, however, may have some importance and our assumption may not be entirely valid at high flow rates. We assumed as an initial condition for the bed consolidation a homogeneous column filled with particles at the minimum density for which they are in contact. At time $t = 0$, the piston is moved forward by a certain distance, or a certain mechanical stress is applied to it. An equilibrium is achieved when the compression resistance of the bed equals this external stress. The model of column proparation studied here includes two steps. During the first step, the excess solvent is extracted from the slurry and a homogeneous mass of packing material is obtained. This mass is consolidated into a heterogeneous bed by the fast mechanical loading of the piston. We studied the effect of this mechanical loading (the displacement of a stress) using a nonlinear elastic-plastic model.

### *Column bed model*

We follow the same general approach as was used by Yuan et al. (1998). A momentum balance for the particle phase is written

$$[\nabla \cdot \sigma] = e_v \nabla P - \rho_s g \tag{1}$$

where $\sigma$ is the stress matrix of the solid phase, $e_v$ is the void fraction (equal to $\epsilon/(1-\epsilon)$ with $\epsilon$ the external porosity of the bed), $P$ is the fluid pressure, $\rho_s$ is the density of the packing material, and $g$ is the gravitation. Equation 1 states the balance between the solid phase stress and the effect of fluid drag and gravity on this solid. In all cases of practical interest in preparative chromatography, gravity is negligible. The pressure gradient can be derived from Darcy law (Bird et al., 1960; Lambe and Whitman, 1979)

$$u_l - u_s = -\frac{k_0 d_p^2}{\epsilon \eta} \nabla P \tag{2}$$

where $u_1$ and $u_s$ are the velocities of the liquid and the solid, respectively, $k_0$ is the permeability coefficient, $d_p$ is the average particle diameter, and $\eta$ is the viscosity of the liquid. The permeability coefficient is related to the void fraction by the Kozeny-Carman equation

$$k_0 = \frac{1}{150} \frac{\epsilon^3}{(1-\epsilon)^2} \tag{3}$$

This system of equations must be completed by a constitutive relationship that relates the applied stress and the deformation of the material (see next section), and by an expression for the shear strength of the interface between the bed and the column wall. In a first approximation, this last condition was omitted by Yuan et al. (1998), who assumed implicitly that the bed never slips against the wall, that is, that the friction between bed and column wall is infinite. Previous experiments have shown that this is not so (Guiochon et al., 1999; Cherrak et al., 2001), and we include in this work the friction and the shear strength, as described in Part I of this article (Yew et al., 2003).

### *Rheology and the nonideal elastico-plastic model*

The mechanical behavior of solid materials under external stress is described by constitutive laws (Desai and Siriwardane, 1984). It is now well understood that we have access to a great variety of materials that may follow quite different constitutive laws. Obviously, the use of an improper constitutive law in a model of mechanical behavior will have results of doubtful validity. Considerable activity is also devoted to the identification of the parameters of the proper constitutive law for each new material. The simplest constitutive law is the linear elasticity of Hooke law that states that the deformation of a compressed element is proportional to the stress and to the length of the element. However, the rheological behavior of most materials is rarely linear (Desai and Siriwardane, 1984) and more complex laws are required for realistic modeling.

The behavior of the packing material in the column was represented by a Frictional Material Model (FMM) that can represent the yielding or failure of the material. This model, developed by Drucker and Prager (1952), is a nonlinear elastic-plastic model which can represent the increase in the yield stress as the mean stress increase. This representation of frictional behavior is important in the modeling of particulate materials. It is not and should not be considered in models commonly used for nonfrictional materials such as metals. These last models, however, are not suitable for the particulate beds studied here. At stresses less than yielding, a nonlinear elastic model was used. The model was first validated by comparing the results with those obtained in the laboratory during the consolidation of the packing material. A simple friction model was used for the contact with the wall and compared with results of shear tests made against a stainless steel plate (Yew, 2000; Yew et al., 2003). Identification of the model solutions allowed the determination of further parameters of this model.

The chromatographic column is enclosed in a stainless steel tube. The behavior of this material during the packing of the column was modeled by assuming it to be elastic, with a Young or elasticity modulus of $2 \times 10^8$ kPa and a Poisson ration of 0.3, typical values for stainless steel (Popov, 1968).

*Elastic Behavior.* In the elastic range, the nonlinear porous elastic material model implemented in ABAQUS (Anon., 1998) was used. In this model, the volumetric strain $\epsilon_{\text{vol}}$ in the material is proportional to the logarithm of the mean stress or equivalent pressure $p = (\sigma_{11} + \sigma_{22} + \sigma_{33})/3$, which is the trace (or the sum of the diagonal terms) in the stress matrix. The volumetric strain of the porous material is related to a parameter $J^{el}$ equal to the logarithm of the elastic volume change (Anon., 1998)

$$e_{\text{vol}} = \ln J^{el}$$

$$J^{el} = 1 + \frac{K}{1 + e_0} \ln\left(\frac{p_0 + p_t^{el}}{p + p_t^{el}}\right) \tag{4}$$

where $K$ is the logarithm of the bulk modulus of the packed bed, $e_0$ is the initial void ratio, $p_0$ is the initial mean stress, and $p_t^{el}$ is the elastic tensile strength of the packing material.

Therefore, $J^{el}$ tends toward infinite when $p$ tends toward $-p_t^{el}$.

Figure 2 illustrates the experimental strain–stress relationships observed (symbols) during the application of the normal stress in the direct shear test (Yew, 2000; Yew et al., 2003), for three different samples of Zorbax. The relationship predicted by the model is also plotted in Figure 2 (line). This relationship was obtained with values of $k = 0.010$, $p_0 = 0.0$ kPa, and $p_t^{el} = 100.0$ kPa, and an assumed value of 0.30 for Poisson's ratio. There is a good agreement between the experimental data and the prediction of using the porous elastic material model.

*Mohr-Coulomb Model.* Inelastic material models are usually not written directly in terms of stress $\sigma$, but in terms of stress invariants, measures of the stress that do not change if the reference coordinate system is changed. These stress invariants will be defined later, in the explanation of the Drucker-Prager (1952) model. It is convenient, however, to refer to the classical Mohr-Coulomb criterion of failure for elastic materials, as a starting point (see Figure 3). This criterion is widely used, and many routine design calculations in soil mechanics and civil engineering are still performed using it.

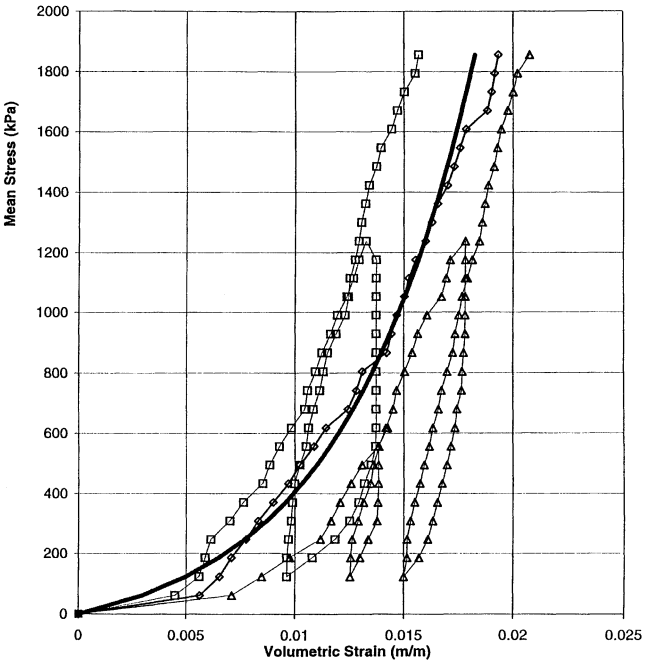


**Figure 2. Mean stress applied to the material vs. the volumetric strain exhibited in the direct shear test (Yew et al., 2003; Yew, 2000).**

Sample: 50 g of Zorbax; see experimental conditions in Yew et al. (2003). Numerical values: $k = 0.010$, $p_0 = 0.00$ kPa, $p_t^{el} = 100.0$ kPa, Poisson ratio = 0.30. Symbols: experimental data, Δ sample 1; □ sample 2; ◇ sample 3. Solid line: porous elastic material model.

The Mohr-Coulomb criterion assumes that failure is controlled by the shear stress and that this failure shear stress depends on the normal stress. This can be represented by plotting Mohr's circle for states of stress at failure. The Mohr-Coulomb failure line is the best straight line that touches these Mohr's circles. Thus, the Mohr-Coulomb criterion can be written as

$$\tau = C + \sigma \tan \phi \tag{5}$$

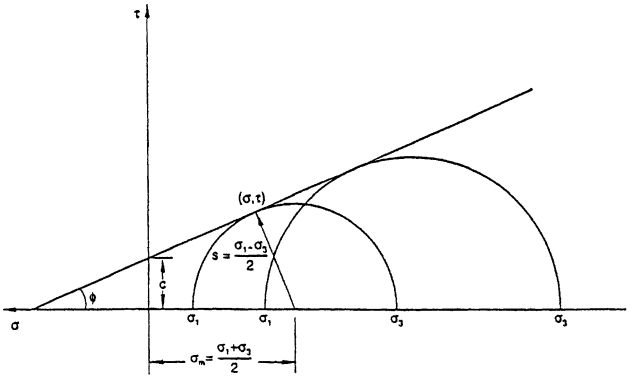


**Figure 3. Mohr-Coulomb failure criterion.**

where $\tau$ is the shear stress at failure or shear strength, $\sigma$ is the normal stress (positive in compression), $C$ is the cohesion of the material, and $\phi$ is the material angle of friction (Figure 3). The traditional coefficient of friction is the tangent of the friction angle. From the properties of Mohr's circle, we have

$$\tau = s\cos\phi = \frac{\sigma_1 - \sigma_3}{2}\cos\phi$$
$$\sigma = \sigma_m - s\sin\phi = \frac{\sigma_1 + \sigma_3}{2} - \frac{\sigma_1 - \sigma_3}{2}\sin\phi \qquad (6)$$

Substituting these values of $\tau$ and $\sigma$ in the Mohr-Coulomb criterion (Eq. 5) and simplifying yields an equivalent expression

$$s - \sigma_m \sin\phi - C\cos\phi = 0$$
$$(\sigma_1 - \sigma_3) - (\sigma_1 + \sigma_3)\sin\phi - 2C\cos\phi = 0 \qquad (7)$$

where $\sigma_1$, $\sigma_3$, and $\sigma_m$ are the maximum principal stress, the minimum principal stress, and the mean normal stress, respectively, and $s$ is the maximum shear stress. Thus, the Mohr-Coulomb criterion assumes that failure is independent of the value of the intermediate principal stress. The failure of typical geotechnical materials (such as a sand heap) generally depends but slightly on the intermediate principal stress, but the Mohr-Coulomb model is usually considered as sufficiently accurate for most applications.

Another way to rewrite the Mohr-Coulomb criterion is as a linear yield function, such that

$$F = \tau - \sigma\tan\phi - C = 0 \qquad (8)$$

If the applied stresses are such that $F = 0$, the material is yielding or can be considered to have failed. If $F < 0$, the material stress state is below yielding. Equation 8 is a generalized expression of the Mohr-Coulomb criterion and provides an easy introduction to the Drucker-Prager (1952) model of constitution law.

*Plastic Behavior.* Most solid, rigid common materials (such as metals) exhibit linear or nonlinear elastic behavior up to yield. All materials yield under stress, but elastic materials return to their initial dimensions when the stress is released, while plastic materials do not. They remain permanently deformed. A very plastic solid, like butter, has no permanent shape and yields under very low stresses. Most geologic materials (particularly sands which are similar to HPLC packing materials for the purpose of this study) yield under stress in a certain range and demonstrate approximate elastic behavior below this range. Theirs is called elastic-plastic behavior (Desai and Siriwardane, 1984; Drucker and Prager, 1952).

*Elastic-Plastic Behavior.* This behavior is the one previously described (Yew et al., 2003) for granulated material under stress. In a certain range of stress, the material exhibits essentially elastic behavior. Beyond a certain threshold, the behavior becomes plastic. The permanent deformation arising from this change may cause hardening of the material and the yield surface expands. Under further loading, the sample will behave elastically in a wider range of stress. Pressure-dependent plasticity models are historically popular in geotechnical engineering. Recently, they have also been found useful for the modeling of some polymeric and composite materials that exhibit significantly different yield behavior in tension and in compression. The linear Drucker-Prager model provides a circular section in the deviatoric $\pi$-plane for the onset of inelastic flow. If a nonassociative flow rule is adopted, different dilation and friction angles result. This model is one of the simplest available for simulating frictional materials. The smoothed surface used in the deviatoric plane differs from a true Mohr-Coulomb surface that exhibits vertices (see Figure 4). This has some restrictive implications, especially with respect to flow localization studies for granular materials, but this may not be of major significance in many routine design applications.

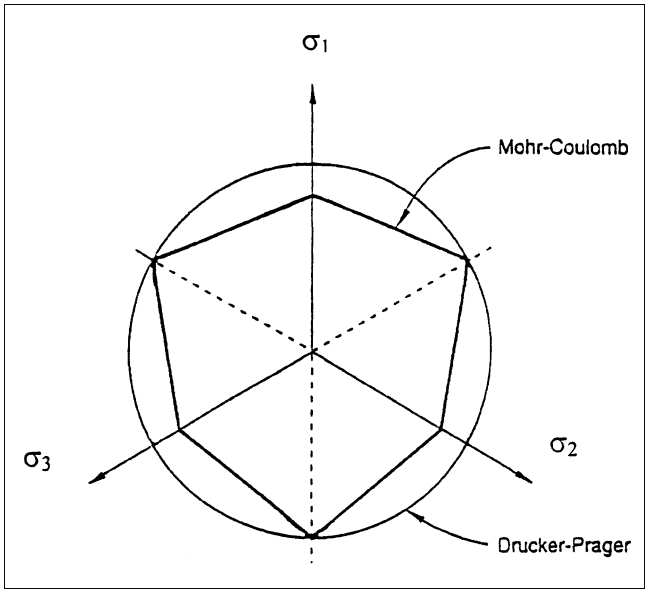


**Figure 4. Mohr-Coulomb model in the deviatoric plane.**

The linear Drucker-Prager model was used to represent the behavior of the packing materials. This constitutive model is an extension of the classical Mohr-Coulomb failure criterion. It is an elastoplastic model that uses a yield function of the Mohr-Coulomb form, including isotropic cohesion hardening/softening. This model uses a flow potential that has a hyperbolic shape in the meridional stress plane and has no corners in the deviatoric stress space. This flow potential is then completely smooth and, therefore, provides a unique definition of the direction of plastic flow.

In this model, the yield surface function $F$ is given by

$$F = q - p\tan\beta - d = 0 \qquad (9)$$

where $\beta$ is the slope of the yield function in the $p - q$ stress space, $p$ is the mean stress, $q$ is the Mises equivalent stress, and $d$ is the yield function intercept on the $q$-axis, as illustrated in Figure 5. We have

$$p = -\frac{1}{3}\,\mathrm{trace}(\sigma)$$
$$q = \sqrt{\frac{3}{2}(S_{ij}S_{ij})} \qquad (10)$$

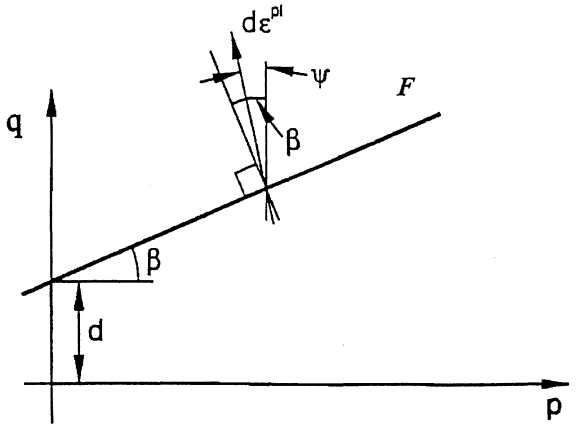


**Figure 5. Linear Drucker-Prager (1952) model yield surface in the meridional plane.**

where $\sigma = \sigma_{11} + \sigma_{22} + \sigma_{33}$ is the sum of the stresses along the three principal axes and $S$ is the deviatoric stress tensor defined as

$$S_{ij} = \sigma_{ij} + p\delta_{ij} \tag{11}$$

Since $q$ and $p$ are related to $\tau$ and $\sigma$, respectively, $\beta$ is related to $\phi$ and $d$ to $c$. Based on the internal friction angle determined independently by Mihlbachler et al. (1998) on similar materials, values of $\beta = 46°$ and $d = 0.73$ kPa were used in the analysis.

*Plastic Flow.* The use of an associative flow rule ($\psi = \beta$) to describe the plastic deformation tends to produce excessive dilation or volume increase during shear (Desai and Siriwardane, 1984). A nonassociative flow rule was used such that a nondilatant response could be represented. This was accomplished by assuming that the dilation angle $\psi$ is equal to zero. The latter means that the plastic deformation is incompressible (there is no plastic volume change as the material deforms plastically). The term $d\epsilon^{pl}$ represents the incremental plastic strain vector, which is normal to the yield surface.

### *Seepage response due to fluid pressure*

The effect of the seepage forces on the density distribution of the column will be evaluated by conducting a numerical simulation of the flow of solvent through the column. As observed by Guiochon and Sarker (1995), Guiochon et al. (1997, 1999) and Cherrak and Guiochon (2001), a chromatographic bed is submitted to a compression stress of two origins. First, in axial compression columns, the piston causes a mechanical compression of the entire bed. This mechanical compression can be modeled numerically as described earlier in the two previous sections. Because there is friction of the bed along the side wall, this mechanical stress is the greatest at the piston edge (bottom) and decreases along the length of the column (see Results and Discussion), as originally demonstrated by Train (1956, 1957). Second, in addition to this mechanical compression, the bed is submitted to a stress originating from the seepage of the mobile phase. The mobile phase stream percolates through the column, because a certain head pressure is applied to the fluid at the column inlet and the fluid flows freely from the column outlet. This results in a pore fluid pressure that decreases along the column and, accordingly, in an increase in the intergranular contact stresses along the column. This may cause some reorientation of the packing material whenever one particle moves or breaks (this explains why columns are sometimes unstable and may consolidate further when the operation conditions change). This stress of seepage origin also interacts with the nonlinear strain-stress behavior of the packing material. Since, due to the flow of mobile phase during the chromatography process, the seepage forces affect the stress state in the packing material, these forces vary with position due to wall friction and the radial inhomogeneity of the packed bed.

*Coupling with Seepage Effects.* A coupled flow and deformation model was developed to further simulate the effects of single-phase flow on the radial heterogeneity of the packed chromatography beds. This coupled analysis is important because the local permeability of the bed of packing material is influenced by the local void ratio, which is, in turn, influenced by the stress state. Since the stress state is influenced by the fluid potential, a coupled analysis is required. This analysis is based on the relationship between permeability and void ratio reported previously (Yew et al., 2003).

Consider a unit volume of a porous media such as that shown in Figure 6 (this unit volume corresponds to the mesh element in Figure 7). This element is usually called an elemental control volume. The law of conservation of mass for the steady-state flow of mobile phase solution through the saturated porous medium requires that the rate of fluid mass flow into any elemental control volume be equal to the rate of fluid mass flow out of this elemental control volume, in the particular case of no retention which is considered here. The equation of continuity that translates this law into the mathematical form that can be written as (Freeze and Cherry, 1979)

$$\frac{\partial(\rho u_x)}{\partial x} + \frac{\partial(\rho u_y)}{\partial y} + \frac{\partial(\rho u_z)}{\partial z} = 0 \tag{12}$$

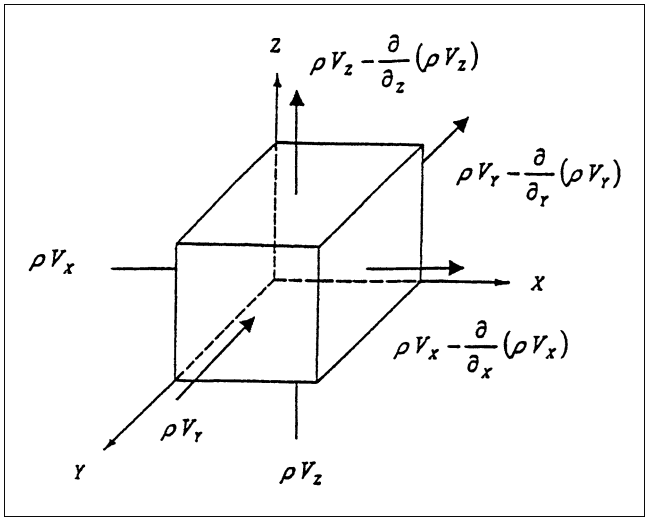


**Figure 6. Element of volume for flow through porous media.**

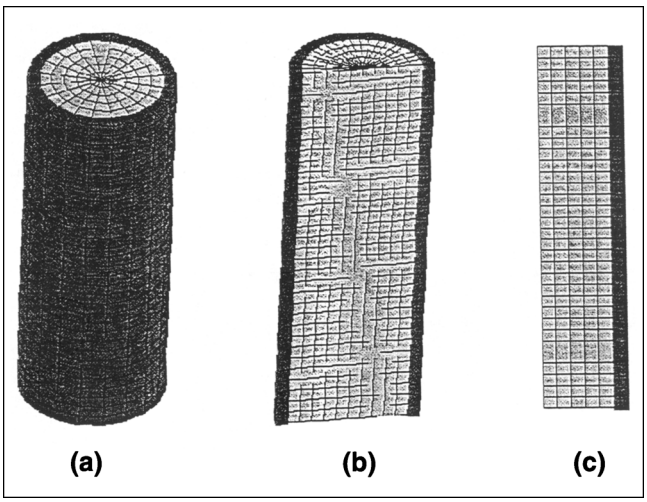


**Figure 7. Discretization of the column bed for calculation purposes.**

(a) 3-D view of the tilted column; (b) representation of the column section; (c) 2-D mesh network used for the actual calculations.

where $\rho$ is the density of the percolating fluid, and $u_x$, $u_y$, and $u_z$ are the velocities (or volumes flow rate of the fluid per unit cross-section area) in the $x$, $y$, and $z$ directions, respectively. Since the compressibility of the fluid is negligible, the density of the fluid $\rho$ can be assumed to be constant and, thus, removed from the equation. Subsequent substitution of Darcy's Law (Bird et al., 1960; Lambe and Whitman, 1979) for $u_i = K_i\ \partial h/\partial x_i$ in Eq. 12 yields the equation for steady-state flow through an anisotropic saturated porous medium (Freeze and Cherry, 1979)

$$\frac{\partial}{\partial x}\left(K_x\frac{\partial h}{\partial x}\right)+\frac{\partial}{\partial y}\left(K_y\frac{\partial h}{\partial y}\right)+\frac{\partial}{\partial z}\left(K_z\frac{\partial h}{\partial z}\right)=0 \quad (13)$$

where $K_i$ is the permeability of the porous medium in the $i$ direction ($i = x,\ y,\ z$) and $h$ is the hydraulic head. If it is assumed that the porous medium is isotropic, then $K_x = K_y = K_z$ and Eq. 13 simplifies to (Freeze and Cherry, 1979)

$$\frac{\partial^2 h}{\partial x^2}+\frac{\partial^2 h}{\partial y^2}=\frac{\partial^2 h}{\partial z^2}=0 \quad (14)$$

Equation 14 is a Laplace equation. It gives the hydraulic head or liquid pressure at any point in a three-dimensional (3-D) homogeneous, isotropic, saturated, steady-state flow field. Steady-state saturated flow assumes a constant flow rate inside the HPLC column during the packing process which can be maintained only if the required pressure excursion remains within the specifications of the pump. The flow rate is controlled by Darcy's Law. This model assumes further that the storage effects due to the compressibility of the packing particles and of the fluid are negligible. While isotropic conditions with respect to the permeability are assumed ($K_x = K_y = K_z$), spacial variation in the permeability is included in the model, based on the variation of the mean stress. Isotropic permeability may not be valid in the immediate vicinity of the wall. This question should be investigated further.

*Transient Analysis.* The law of mass conservation for transient flow in a saturated porous medium requires that the net rate of fluid mass flow into any elemental control volume be equal to the time rate of change of the fluid mass stored within the element. The fluid mass stored within a volume element can be characterized by the specific storage $S_s$ or volume of fluid released from a unit volume of saturated porous medium for a unit decline in the hydraulic head $h$

$$S_s = \rho g\left(\alpha_{pm}+\epsilon_T\beta_w\right) \quad (15)$$

where $\rho$ is the fluid density, $g$ is the gravitational acceleration, $\alpha_{pm}$ is the compressibility of the porous medium, $\epsilon_T$ is its porosity, and $\beta_w$ is the compressibility of the fluid. Because of this definition, $S_s$ is not an implicit function of time. During column consolidation, $\alpha_{pm}$ and $\epsilon_T$ decrease slightly. The variation is small, however, and we assume in the following that $S_s$ remains constant.

The mass balance of the fluid is no longer given by Eq. 12 which applies to steady-state, but by the following equation (see Figure 6) (Freeze and Cherry, 1979)

$$\frac{\partial(\rho u_x)}{\partial x}+\frac{\partial(\rho u_y)}{\partial y}+\frac{\partial(\rho u_z)}{\partial z}=\frac{\partial(\epsilon\rho)}{\partial t} \quad (16)$$

The righthand side of this equation can be expanded and simplified by substituting the time rate of change of the fluid mass stored, $\rho S_s\partial h/\partial t$

$$\frac{\partial(\rho u_x)}{\partial x}+\frac{\partial(\rho u_y)}{\partial y}+\frac{\partial(\rho u_z)}{\partial z}=\rho S_s\frac{\partial h}{\partial t} \quad (17)$$

The terms on the lefthand side of this equation are expanded by the chain rule. Further simplification is carried out by recognizing that the terms of the form $v_x\partial\rho/\partial x$ are insignificant compared to terms of the form $\rho\partial v_x/\partial x$ and by removing the former from the equation, by eliminating $\rho$ from both sides, and by substituting Darcy's Law. These manipulations yield the equation for transient flow through a fully saturated, anisotropic, porous medium (Freeze and Cherry, 1979)

$$\frac{\partial}{\partial x}\left(K_x\frac{\partial h}{\partial x}\right)+\frac{\partial}{\partial y}\left(K_y\frac{\partial h}{\partial y}\right)+\frac{\partial}{\partial z}\left(K_z\frac{\partial h}{\partial z}\right)=\frac{S_s}{K}\frac{\partial h}{\partial t} \quad (18)$$

If it is appropriate to assume that the slurry in HPLC columns is homogeneous and isotropic prior to the packing process, the equation can then be simplified into (Freeze and Cherry, 1979)

$$\frac{\partial^2 h}{\partial x^2}+\frac{\partial^2 h}{\partial y^2}+\frac{\partial^2 h}{\partial z^2}=\frac{S_s}{K}\frac{\partial h}{\partial t} \quad (19)$$

In summary, transient saturated flow assumes that the rate of flow changes with time inside HPLC columns during the packing process. This is certainly the case of columns packed by slurry filtration (Guiochon et al., 1997). The flow rate of

packing solvent is then controlled by Darcy's Law and by the storage effect due to the compressibility of the packing material (and, to a minor degree, to that of the solvent).

### *Calculation of numerical solutions*

The integration of the system of partial differential equations modeling the behavior of the column bed is impossible. As in many cases of importance in engineering, analytical solutions are not available. However, the calculation of numerical solutions of this system in practical cases is possible with techniques such as the finite element method (FEM), which gives the stress-state inside HPLC columns during the packing process (Cook, 1995). The FEM is a collection of theory-rich techniques which can produce near-optimal approximate solutions to the initial-boundary value partial differential equations common to engineering and mathematical physics (Baker and Pepper, 1991). The stress distribution in a typical preparative HPLC column was investigated using the commercial, general-purpose finite-element code ABAQUS, version 5.8 (1998) (Anon, 1998). The material parameters used in the analysis were obtained from the laboratory testing [Yew et al., 2003]. The numerical results from ABAQUS were evaluated via the post processing package, ABAQUS/Post (1998), which generated the graphical results (Anon., 1998).

In the finite-element method, it is assumed that the element size, although finite, is small enough to legitimize the replacement of all functions considered in the calculation by their average in the element and to neglect the extent of their variations within the element. As the number of elements increases, a proper finite-element solution should converge toward the analytical or exact solution of the set of differential or partial differential equations that express the mathematical model. However, theorems of existence of an analytical solution to the problem, let alone of the convergence of a numerical solution toward this analytical solution, are usually lacking. Thus, the convergence of a numerical solution, such as a finite-element one, can be evaluated only on the assumption that all basic kinematic, static, and constitutive conditions contained in the mathematical model must ultimately be satisfied at the convergence. Thus, in all further discussions of the convergence of the finite-element solution, we imply convergence toward the exact solution of the mathematical model.

To model an HPLC column, a 3-D model should be used. However, due to the axisymmetric nature of the column and of the packing process, it is reasonable to simplify this model and to consider only a 2-D model, as illustrated in Figure 7. In the calculation, four-node linear axisymmetric continuum elements were used. Contact elements with the desired coefficient of friction were used to represent the frictional surface between the bed and the steel wall.

It is important to find an acceptable compromise for the size of the elements, between the use of too coarse or too small ones. The former would introduce important numerical errors and an unacceptable deviation of the numerical solution from the exact one. The latter would result into excessively long run times. For monotonic convergence, the elements must be complete and the elements and the mesh size must be compatible. If these conditions are fulfilled, the accuracy of the solution should increase continuously with decreasing size of the finite-element mesh. However, below a certain range, decreasing the element size does not bring an improvement in the accuracy of the numerical solution that would be warranted, given the approximations made in designing the model and in determining the numerical values of its parameters. The mesh refinement is usually performed by subdividing a previously used element into two or more elements. So, the old mesh is embedded into the new, smaller mesh. Mathematically, this means that the new space of the finite-element interpolation functions will contain the previously used space and that, as the mesh is refined, the dimension of the finite-element solution space increases continuously to contain ultimately the exact solution.

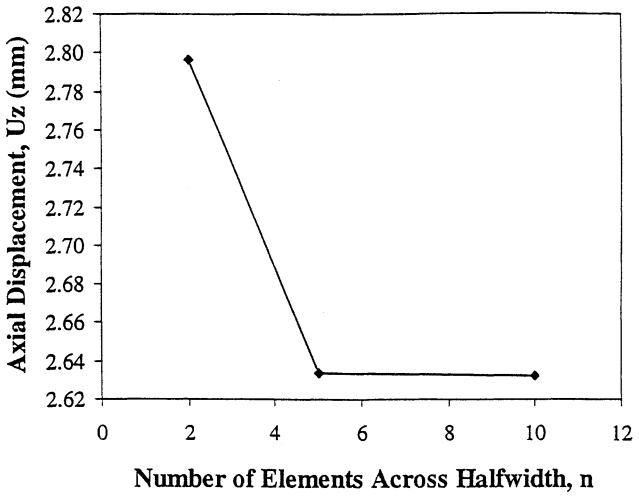


**Figure 8. Convergence of the axial displacement at point A (Figure 7) in the column toward its limit with increasing number of elements across the column radius used in the calculation of the finite-element solution.**

To investigate the convergence of the numerical solution of the model used for preparative HPLC columns, a series of successive computations were performed with two, five, and ten elements across the half-width of the column (for a total of 4, 10, and 20 coaxial cylinders, respectively, see Figure 7b). The axial displacements were measured at point A along the column wall and point B on the column axis, in places where the displacement is still important, but which are far enough from the piston head at which the displacement is known, since it is a boundary condition. The displacement observed is plotted vs. the number of elements along the column radius in Figure 8. This figure shows that two was an insufficient number of elements while there is very little difference in the displacements calculated with five and ten elements. Therefore, all further calculations were conducted with five elements in the radial direction. The same nodal spacing was adopted in the axial direction to produce square elements.

The FE method calculates first the nodal displacements from which it derives the strains and finally the stresses. Some results are presented as maps of these parameters showing contour lines along which the value of the selected parameter is constant and grey bands of different densities. Others are reported as plots of the stress or strain along the axial or radial distance.

### *Parameters and convergence criteria in the transient analysis*

In ABAQUS, a transient coupled mechanical-seepage analysis is performed when the CONSOLIDATION parameter is included in the *SOILS option (Anon, 1998). In the transient case, the backward difference operator is used to integrate the continuity equation. This operator provides unconditional stability, so the only concern with respect to time integration is the accuracy (Anon., 1998). The integration procedure used for the consolidation analysis introduces a relationship between the minimum usable time increment and the element size, as shown below for fully saturated flows. Provided the time increment is sufficiently large, a unique solution will be obtained. If time increments smaller than these values are used, spurious oscillations may appear in the solution. These oscillations are nonphysical artefacts and may cause problems if pressure-sensitive plasticity is used to model the porous medium (Anon, 1998). If the problem requires analysis with smaller time increments than the relationships given below allow, a finer mesh is required. Generally, there is no upper limit on the time step except that arising from the accuracy required, since the integration procedure is unconditionally stable unless nonlinearities cause convergence problems (Anon, 1998).

A simple empirical guideline that can be used for the minimum usable time increment in the case of fully saturated flow is (Anon, 1998)

$$\Delta t > \frac{Y_w(1+\beta_F u_w)}{6Ek}\left(1-\frac{E}{K_g}\right)^2 \Delta l^2 \qquad (20)$$

where $\Delta t$ is the time increment, $Y_w$ is the specific weight of the liquid, $E$ is the Young's modulus of the porous material, $k$ is its permeability, $u_w$ is the velocity of the fluid, $\beta_F$ is the velocity coefficient in Forchheimer's flow law, $K_g$ is the bulk modulus of the solid grains, and $\Delta l$ is the typical element dimension. When Darcy's law is valid, the velocity coefficient in Forchheimer's flow law $\beta_F$ is assumed to be zero. Furthermore, we assumed the bulk modulus of the solid grains $K_g$ to be infinite because we considered the particles of the packing material to be fully incompressible relative to the compressibility of the packing material. Thus, Eq. 20 simplifies to (Anon, 1998)

$$\Delta t > \frac{Y_w}{6Ek}\Delta l^2 \qquad (21)$$

For the HPLC column finite-element mesh shown in Figure 7, $\Delta l = 0.005$ m, $Y_w = 7.75$ kN/m$^3$, $k = 3.53\times10^{-2}$ m/day, and $E = 1{,}300{,}000$ kPa. This results in $\Delta t = 7.0\times10^{-8}$ day or approximately 6 ms. Finally, we assumed that the maximum pore pressure that was allowed to dissipate in each time increment was UTOL = 1,300 kPa (13.0 bar), which is about 10% of the initial pore pressure. In addition to the convergence criteria discussed above, a maximum rate of pore pressure dissipation over time during each time step is required in the transient analysis toward steady state, in order to describe the maximum rate of pore pressure dissipation. However, the packing material studied here has a relatively high permeability, so this type of numerical solution would stop when the flow reaches a steady-state condition, usually before the intended piston displacement is achieved. Therefore, this type of analysis was not fully investigated.

## Experimental Conditions

The HPLC column considered in this work is a 16.0 cm long, 5.0 cm ID column, similar to those previously studied in this group (Farkas et al., 1997; Guiochon et al., 1997; Guiochon and Sarker, 1995; Sarker et al., 1996; Yun and Guiochon, 1997) and typical of those used in laboratory-scale applications of preparative chromatography. This column was assumed to be packed with Zorbax C18 (BTR Separations, Wilmington, DE, now Agilent Technologies, Palo Alto, CA). It takes approximately 200 g of Zorbax to pack the column considered. The values of the parameters used in this work were determined in an earlier work (Yew et al., 2003). The friction coefficient at the wall was tan $\delta = 0.39$ for Zorbax and 0.21 for Kromasil. The internal friction angles were, respectively, 21.3 and 11.9 degrees. The behavior of the bed obtained was systematically investigated, using all possible sets of experimental conditions. The piston head was assumed to be flat, perpendicular to the column axis.

In the finite-element simulation, a vertical constraint was imposed on the top of the column (which is, thus, unable to move), while a uniform vertical displacement is applied along the bottom of the column bed corresponding to the vertical movement of the rigid piston. This uniform displacement is applied in a stepwise or incremental manner, and the nonlinear analysis is performed at each step to obtain the displacements, strains, and stresses throughout the column corresponding to the new equilibrium conditions. A uniform displacement loading condition was chosen for the numerical analysis because the distribution of stress and deformation in the packing material depends upon the rigidity of piston. For example, a perfectly flexible piston (or a membrane) would impart a uniform distribution of stress on the packing material, but the resulting displacement would vary across the piston. Conversely, a perfectly rigid piston would impart a uniform displacement on the packing material across the piston, but distribution of stress across the piston (which is the desired output in our problem) would vary.

Thus, a uniform displacement boundary condition was utilized in the simulation since this condition most closely approximates the loading from a relatively rigid piston, and the computed stresses, which vary with position in the column, were obtained. This simulated loading in the numerical model is somewhat opposite to the manner in which a physical laboratory column is packed, where a pressure is applied to the piston and the resulting displacement measured. In an actual bed of Zorbax (Guiochon et al., 1999), the application of a mean compression pressure of approximately 10.0 MPa spread uniformly over the outside cross-section of the piston resulted in a piston displacement of about 3.4 mm. Likewise, if a mean pressure of only 6.0 MPa was applied to the piston, about 2.8 mm of piston displacement occurred. Figure 9 illustrates results from the finite-element simulation for these applied displacements of 2.8 mm and 3.4 mm, shown with the corresponding maximum value of mean stress or pressure which is observed to take place at the edge of the piston (see

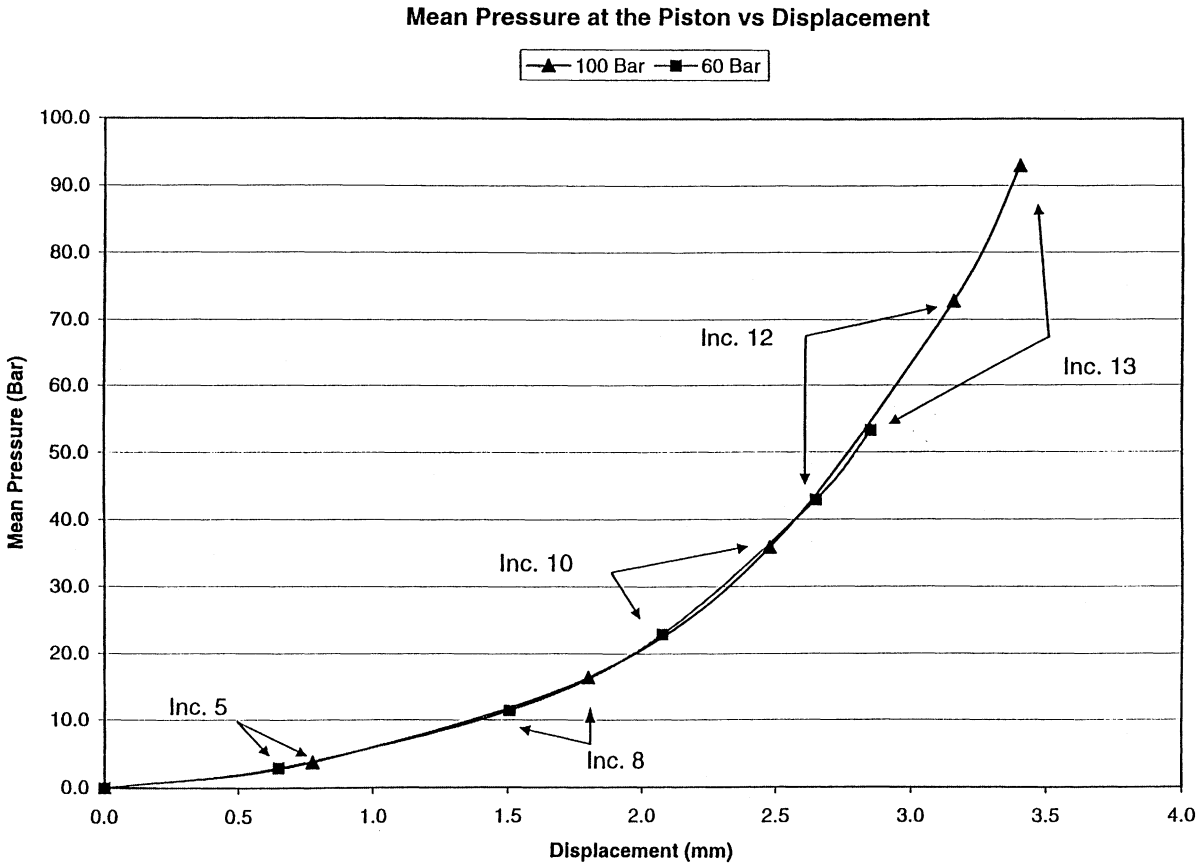


**Figure 9. Behavior of the packing material under stress.**

Computed maximum values of the mean pressure near the edge of the piston vs. the piston displacement, for two simulated laboratory loading cases: a test with an applied piston pressure of about 10 MPa, which experienced 3.4 mm of piston displacement, and a test with an applied piston pressure of about 6 MPa, which experienced 2.8 mm of piston displacement. For the 10 MPa test, the computed maximum value of the mean stress was 9.2 MPa under the imposed piston displacement of 3.4 mm. For the 6 MPa test, the maximum computed stress was 5.3 MPa under the imposed displacement of 2.8 mm.

subsequent discussion of results). For both the maximum applied displacements of 2.8 mm and 3.4 mm, intermediate results corresponding to lesser incremental displacements are also shown. For example, the results for a maximum displacement of 3.4 mm produced intermediate increments of the piston displacement and maximum mean stress of 0.78 mm (0.38 MPa), 1.8 mm (1.6 MPa), 2.48 mm (3.6 MPa), 3.15 mm (7.3 MPa), and 3.4 (9.3 MPa). As expected, the results for the 2.8 mm simulation coincide with those from the 3.4 mm displacement, since the nonlinear stress displacement response is unique based on the selected material model. The maximum values of computed mean pressure for the two loading cases (5.3 MPa for a piston displacement of 2.8 mm and 9.3 MPa for a displacement of 3.4 mm) correspond reasonably well with the simulated piston pressures of 6.0 MPa and 10.0 MPa, respectively. It should be kept in mind that the experimental values of 10.0 and 60 MPa are approximate pressures averaged over the outside of the piston, while the maximum mean pressures of 9.3 and 5.3 MPa are computed values inside the column near the column wall. The computed pressures (and comparison with the physical experiment) could be changed by varying the parameters used in the material model, but the intent was to predict the response using the parameters measured in the laboratory.

Recently, various phenomena taking place inside chromatographic columns were visualized (Broyles et al., 1998, 1999a,b; Shalliker et al., 2000a,b). The method rests on the possibility to pack a chromatographic column in a hard glass tube, using a stationary phase (YMC C18 silica, 30 $\mu$m particles, Kyoto, Japan) and a mobile phase (carbon tetrachloride) that have the same refraction index. The column is then placed in a rectangular box with glass windows, filled with the mobile phase. What takes place inside the column can be seen easily and photographed when needed. The main limitations arise from the limited range of pressures and stress which can be reached inside the glass tube. Viscous fingering was easily illustrated (Broyles et al., 1998). The influence of various parameters on the migration of bands of iodine was investigated (such as flow velocity, frit parameters, and distributor characteristics) (Broyles et al., 1999a,b). Local, nearly point-size injections of iodine made at different locations of the cross-section at the column inlet allowed the measurement of the axial and radial dispersion coefficients and confirmed the existence of two wall effects (Shalliker et al., 2000a,b).

In the present study, thin (about 0.5 mm) layers of an alumina (50 $\mu$m particles from Cohesive Technologies, Franklin, MA) slurry were placed inside the column between succes-

sive thick (about 1 cm) layers of a slurry of the YMC C18 silica that were carefully laid down making sure that their top was flat. Since the alumina particles have a refractive index that is different from those of the silica particles and of carbon tetrachloride, the alumina layers are visible and serve as marker layers. Their photographs after consolidation of the bed (see later) illustrate the differential movements that take place inside the column bed during its axial compression, that is, they illustrate the strain distribution in the bed.

## Results and Discussion

As previously discussed, Figure 9 illustrates the relationship between the piston displacement and the computed values of maximum mean stress at the edge of the piston, for applied maximum displacements of 2.8 mm and 3.4 mm (the corresponding average compression stress are approximately 6 and 10 MPa). Because the maximum displacement is applied in 13 successive increments, intermediate results, as well as the full nonlinear response, are obtained. Only the results obtained after steps 5, 8, 10, 12, and 13 are shown in the figure, for the sake of clarity. Because of the unique stress strain relationship for the packing materials, the two sets of results coincide. Although in the analysis method the computed stresses are obtained as a function of applied displacement, the subsequent discussion of the results is facilitated if described as though the physical experiment was being conducted, with a pressure applied and the resulting displacements and stresses observed.

### *Consolidation without seepage*

Typical results of the calculations made for a column packed under static conditions, with a slurry of Zorbax in methanol are shown in Figures 10 to 14. Figures 10a and 10b show contour maps of the spatial distributions of the local mean stress, the local axial displacement, and the local void ratio across the bed, after completion of upward movements of the piston of 1.5 mm (Figure 10a) and 3.4 mm (Figure 10b), which correspond to mechanical compression stresses equivalent to maximum mean pressures of 1.0 and 9.3 MPa applied to the piston head. The calculated results regarding the distributions of the mean pressure and the displacements are in excellent qualitative agreement with the experimental data of Train (1956, 1957) in this compression stress range. They show that, while most of the column bed is very close to radial homogeneity, the two ends of the column are highly heterogeneous. A wedge region, at the corner of the wall and the piston, is most strongly affected (Figure 10b). The intensity of the effect and the volume of the region most affected increase with increasing compression stress. At high stress (Figure 10b), the top of the column also is affected. The distribution of displacements indicates the effect of wall friction on the displacement field. For any given location along the column axis, the displacement at the center line is greater than that along the wall. The region of high stress at the edge of the rigid piston is analogous to the high contact stresses under the edge of a rigid die of a footing in contact with the ground surface (Lambe and Whitman, 1979).

From a chromatographic perspective, the radial variation of the void ratio is the most important consequence of the bed consolidation that we should consider. The void ratio has a strong influence on the performance of the column, because the local void ratio controls the local permeability that determines the local flow velocity. It is obvious in Figures 10a and 10b that the void ratio varies significantly in both the radial and the axial directions in the vicinity of the piston and in that of the top flange closing the bed at its top. The data in these figures give the big picture. It is useful to complete them by examining axial (Figures 11a and 11b) and radial (Figures 12a–12c) distributions of the void ratio, axial and radial distributions of the compression stress inside the bed (Figures 13a–13e) and axial distributions of the contact shear, contact pressure and contact slip (Figures 14a–14d).

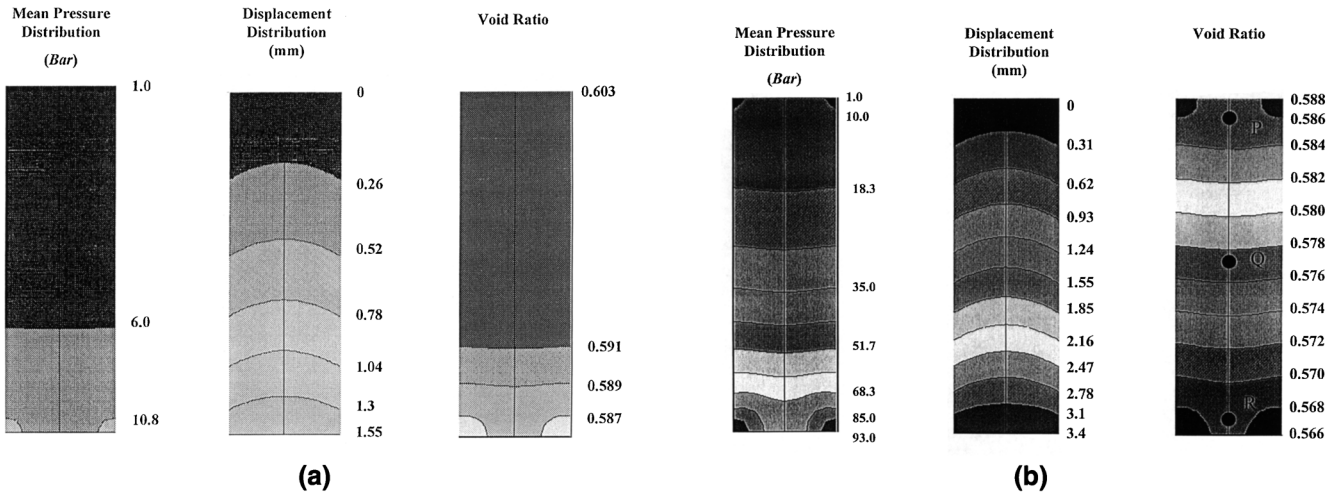


**Figure 10. Contour distributions of the mean mechanical stress, local displacement, and void fraction calculated for a bed packed with a slurry of Zorbax in methanol.**

(a) Compression for the 6 MPa test, increment 8 (corresponding maximum computed stress, 2 MPa); (b) compression for the10 MPa test, increment 13.

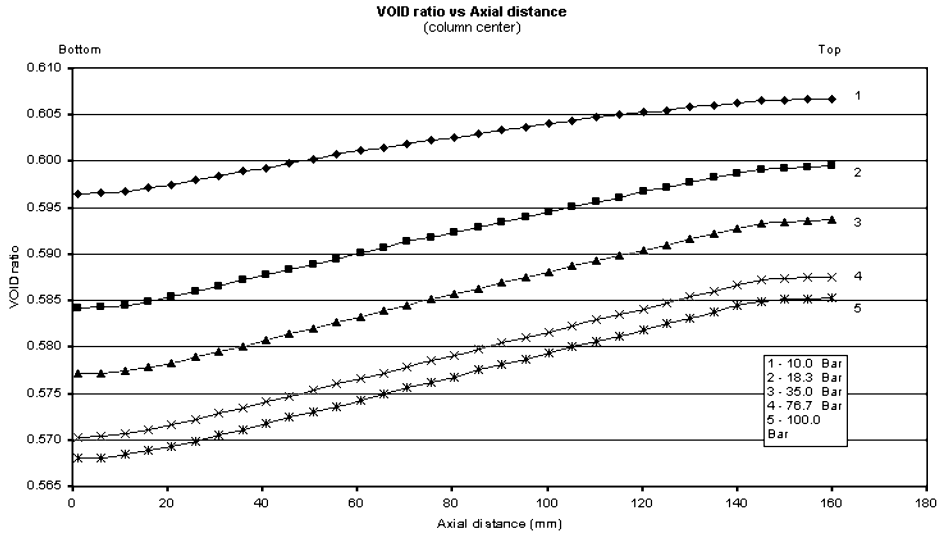


**(a)**

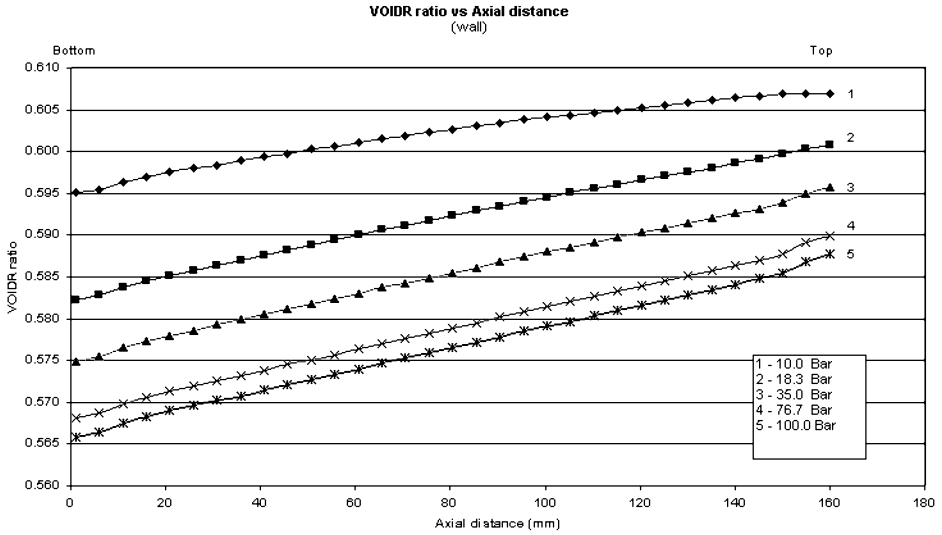


**(b)**

**Figure 11. Axial distribution of the local void ratio (abscissa origin at the piston).**

Axial compression under stress increasing stepwise from 0 to 10.0 MPa. Stress applied to the piston: 1, 1.0 MPa; 2, 1.8 MPa; 3, 3.5 MPa; 4, 7.6 MPa; 5, 10.0 MPa (see Figure 9). (a) Distribution along the column axis; (b) distribution in the axial direction, along the column wall.

*Distributions of the Void Ratio.* Figures 11a and 11b show plots of the axial distribution of the local void ratio along the column axis and against the wall, respectively, for different values of the compression stress. The curves labeled 1 to 5 in these two figures show the axial and radial distributions of the local void ratio under increasing compression stress, that is, its variation during the loading process. The two series of curves are markedly different, although they both exhibit very similar nearly-linear increases in the central region of the column, consistent with the quasi radial homogeneity of the column in this region (a region that includes approximately 75% of the column length). In the top and bottom 10%, however, the axial variations are different in the center and along the wall. The void ratio, hence, the external porosity of the bed, is higher close to the column top. At both ends, the void ratio in the center of the column becomes nearly constant. Along the column wall, by contrast, the variation is significant and, when the compression stress is high, this variation can become steep. This observation is confirmed by the data in Figures 12a to 12c that illustrate the radial variation of the void ratio close to the column top (Figure 12a), in the column center (Figure 12b), and close to the piston (Figure 12c). In the column center, the column is radially homogeneous, as suggested by the data in Figure 10. At the bottom of the column, the void ratio is higher in the core region than in the wall region. In contrast, at the column top, it is higher close to the column wall than along its axis. Although the axial variation of the void ratio may seem small, the very strong

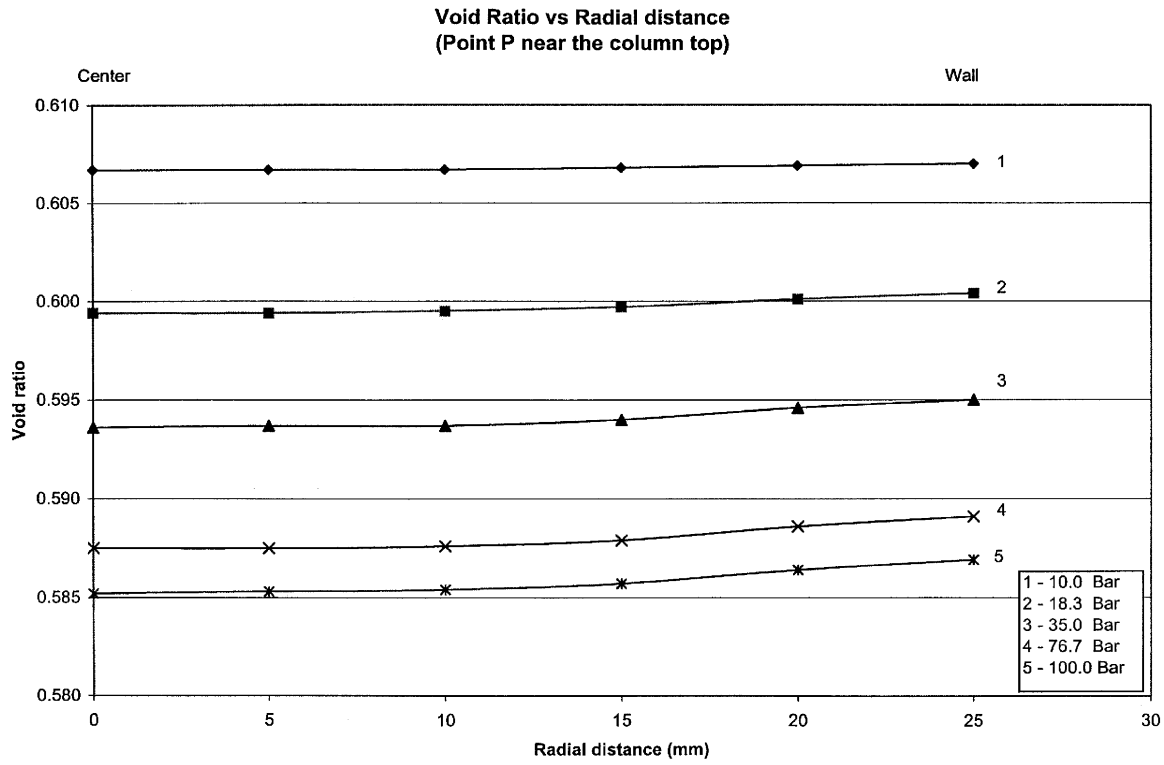


(a)

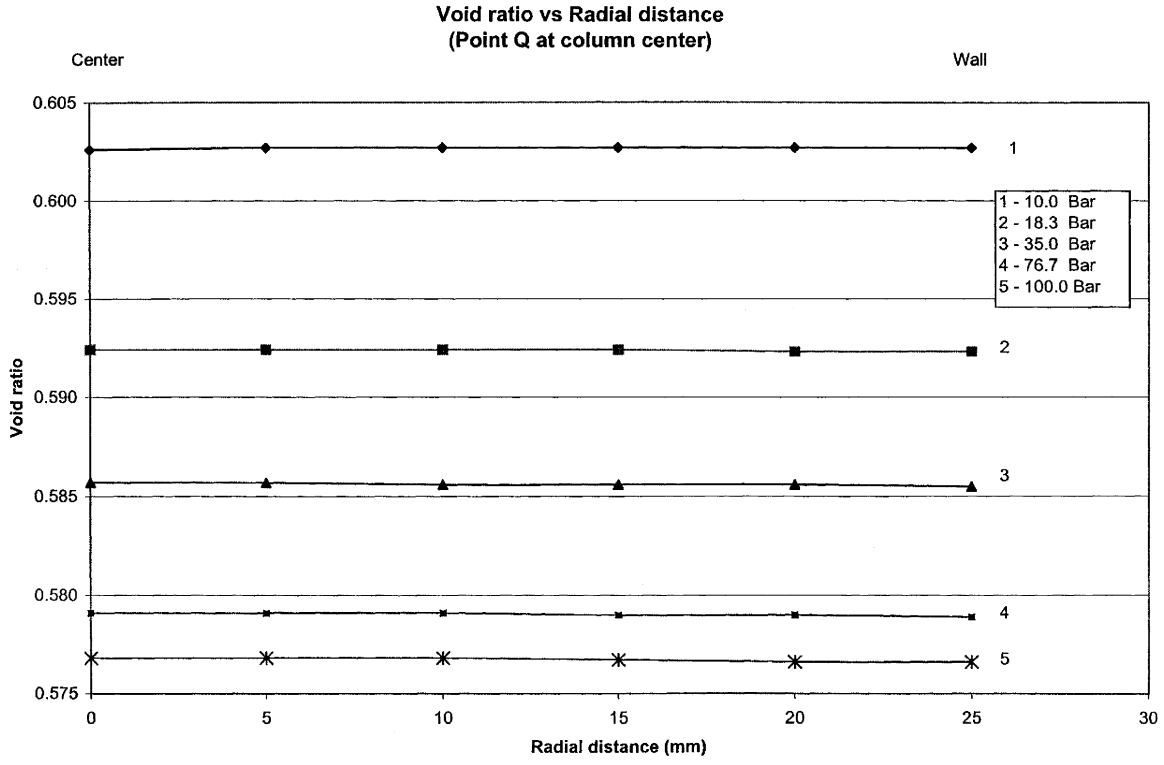


(b)

**Figure 12a,b. Radial distribution of the local void ratio (abscissa origin at the column center) for different values of the axial stress, as in Figure 11.**

(a) Distribution close to the column top, at 5 mm below; (b) distribution in the column center.

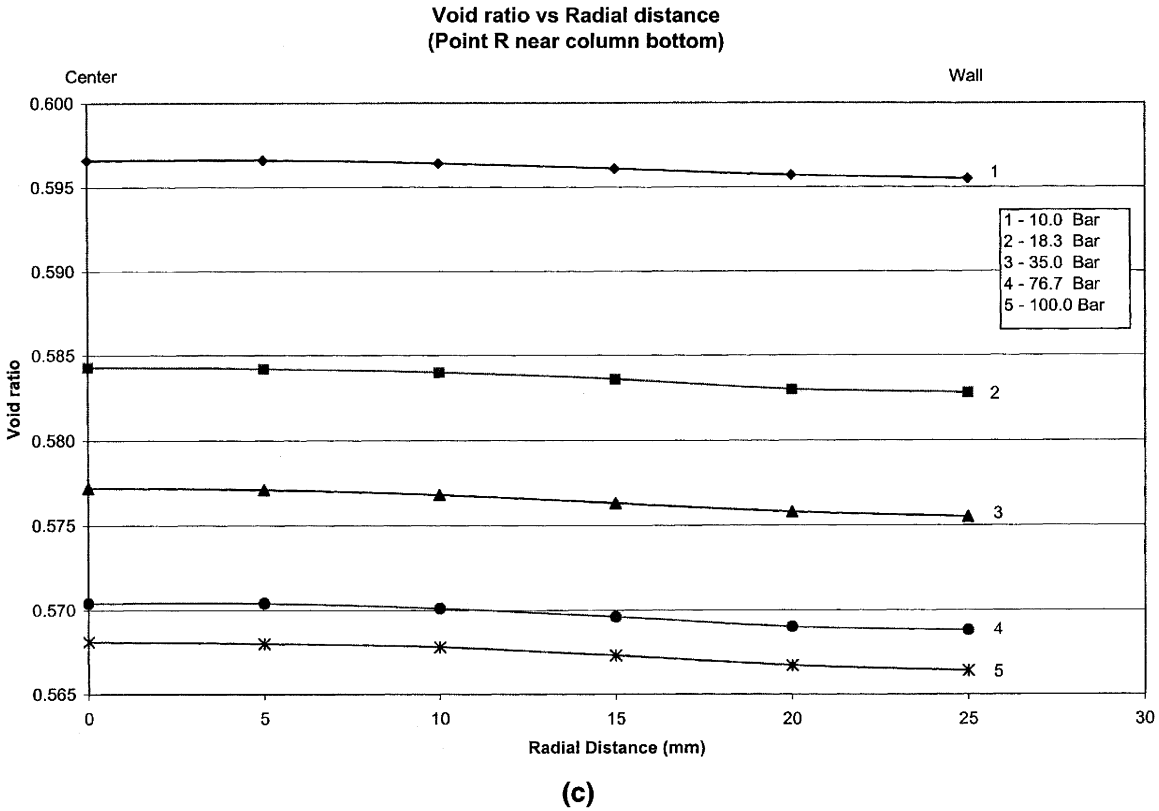


**Figure 12c. Radial distribution of the local void ratio (abscissa origin at the column center) for different values of the axial stress, as in Figure 11.**

(c) distribution close to the piston, 5 mm from it into the bed.

dependence of the permeability on the external porosity (Eq. 3) explains why the influence of this void-fraction variation on the column efficiency causes enough warping of the bands drastically to affect column efficiency.

*Distributions of the Shear Stress.* Figures 13a to 13e show the axial distribution of the shear stress along the column axis (Figure 13a) and against the wall (Figure 13b), and the radial distributions of the shear stress at the bottom of the bed ($z = 10$ mm, Figure 13c), in the bed center ($z = 80$ mm, Figure 13d), and at the top of the column ($z = 150$ mm, Figure 13e). As in the previous figures, the results are shown for increasing levels of mean stress. The shear stress increases rapidly from the center of the column toward the wall (Figures 13c–13e). It increases steeply in the region just above the piston and decreases rapidly in the vicinity of the bed top.

*Distributions of the Contact Stress.* Figures 14a to 14d show the axial distribution of the local contact shear stress (Figure 14a), the contact normal pressure (Figure 14b), the ratio of the contact shear stress and normal pressure (Figure 14c), and the contact slip displacement (Figure 14d). The contact shear stress is the shear stress at the wall. The contact normal pressure is the normal stress applied by the bed against the wall. Both the contact shear stress and the normal pressure are maximum inside the bed, at a short distance above the piston, and decrease continuously toward the top of the bed, falling sharply to zero at its very top, within approximately 5 mm (that is, within one mesh element). Their ratio (Figure 14c) is constant and equal to the friction coefficient along most of the bed which implies that, in this zone, the packing material is slipping relative to the wall. At the top of the bed, the contact shear decreases faster than the contact pressure and their ratio becomes lower than the friction coefficient, indicating that there is no slip in this upper part of the bed. The part of the bed which is not affected by the consequences of slip is small, however, barely the top 10%, except at the lowest displacement increment (curve 1). Finally, the slip decreases uniformly along the bed, until close to the top (Figure 14d).

*Conclusion.* The most important conclusion of these results is that the consolidation by axial compression of a column packed with a particulate material cannot but result in a heterogeneous bed, and that the bed heterogeneity takes place both in the radial and the axial directions. The distributions of the displacements and of the stress are in excellent qualitative agreement with previous results obtained by Train (1956, 1957) in the consolidation of pellets of hydrated basic magnesium carbonate in a die. Complex stress and strain patterns were observed. Within the compression stress range below 7 MPa in which the particles of this material are not damaged, Train (1956, 1957) found that the stress in the region at the bottom of the die was markedly lower than the stress applied on the punch, while stress higher than that was observed in the region close to the punch and the die wall. In

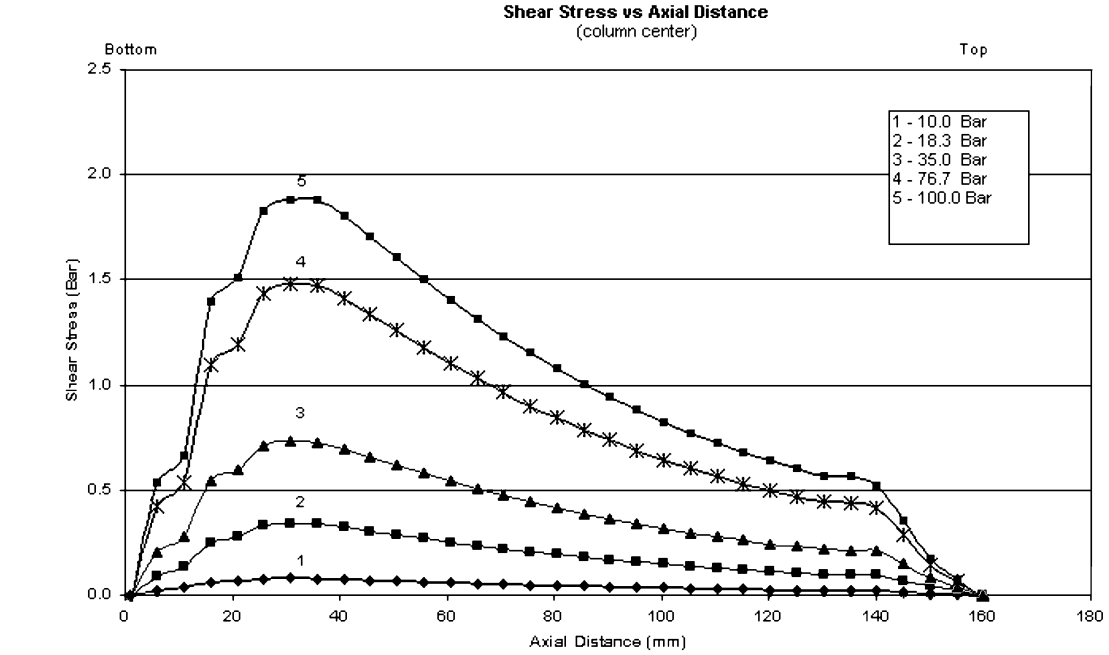


**(a)**

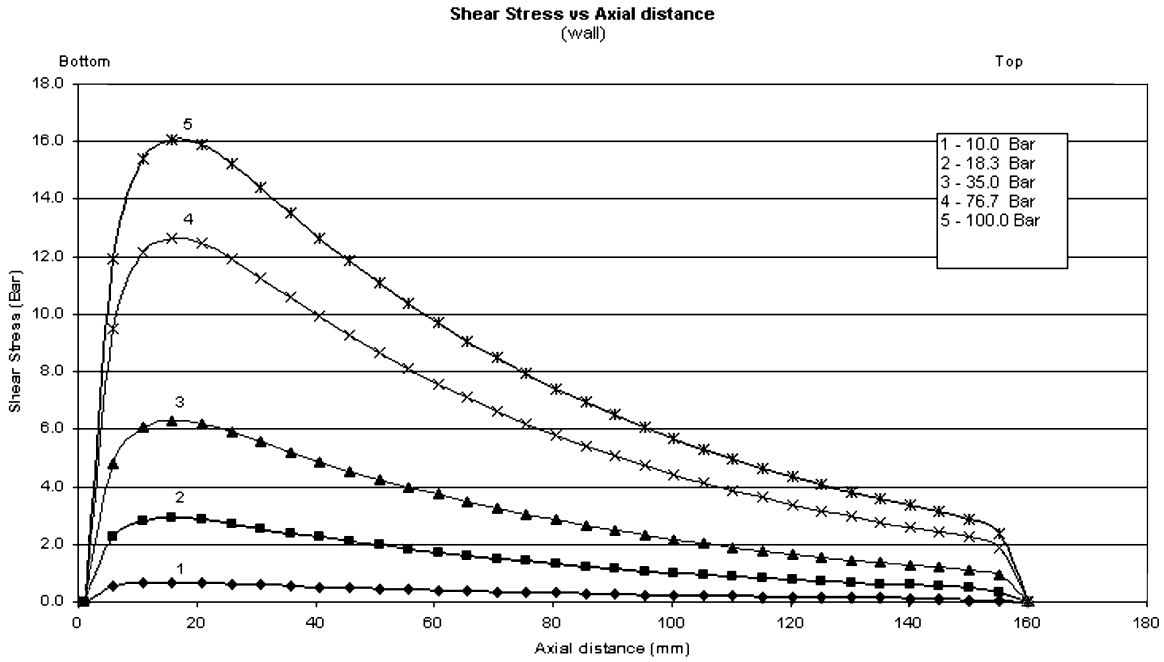


**(b)**

**Figure 13a,b. Distributions of the stress and strain (abscissa origin at the column axis or at the piston), at both ends of the bed and in its center.**

(a) Axial distribution of the shear stress in the column center; (b) axial distribution of the shear stress against the column wall.

agreement with these results, we found in Figures 10 and 13 that there is a concentration of high mean stress in the region of the bed close to the piston and near the column wall. In this region, the local stress calculated significantly exceeds the average mechanical stress assumed to be applied homogeneously over the cross-section of the piston. In this region also, the void ratio is markedly lower than everywhere else (Figure 11b), causing a significant decrease of the local permeability in these regions. This effect is probably sufficient to explain the heterogeneous radial distribution of the outlet ve-

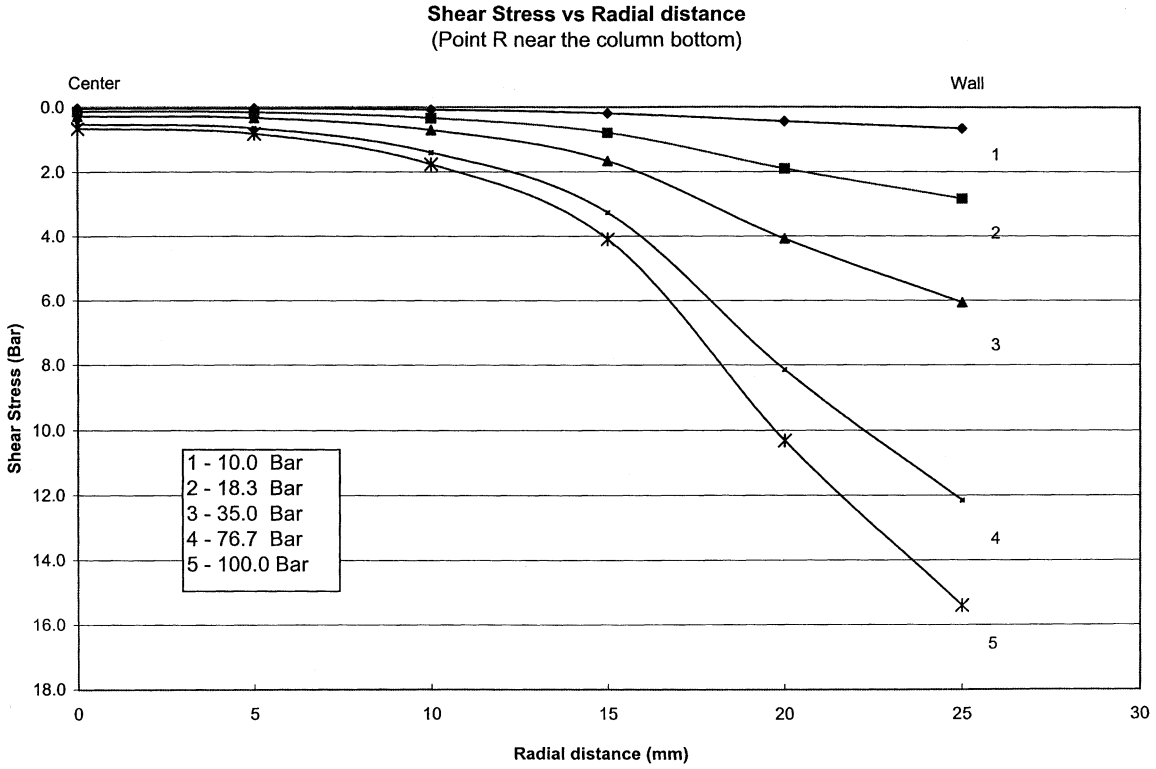


**(c)**

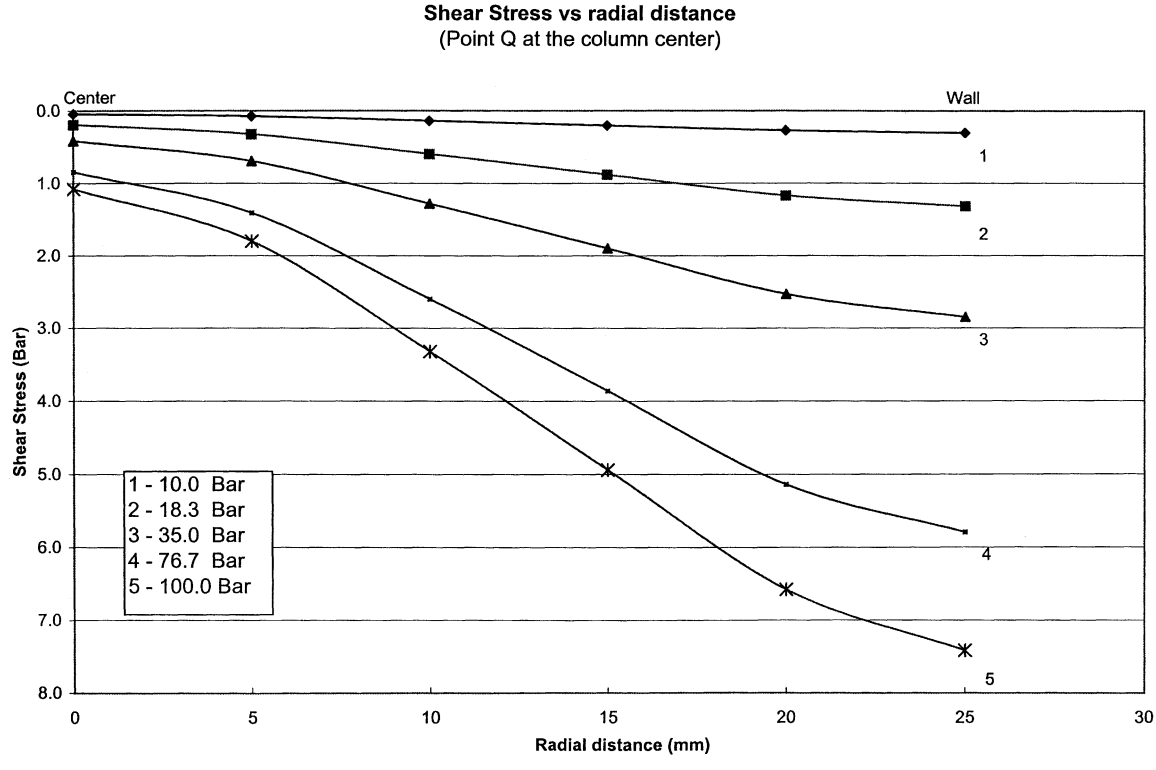


**(d)**

**Figure 13c,d. Distributions of the stress and strain (abscissa origin at the column axis or at the piston), at both ends of the bed and in its center.**

(c) radial distribution of the shear stress at $z = 10$ mm; (d) radial distribution of the shear stress at $z = 80$ mm.

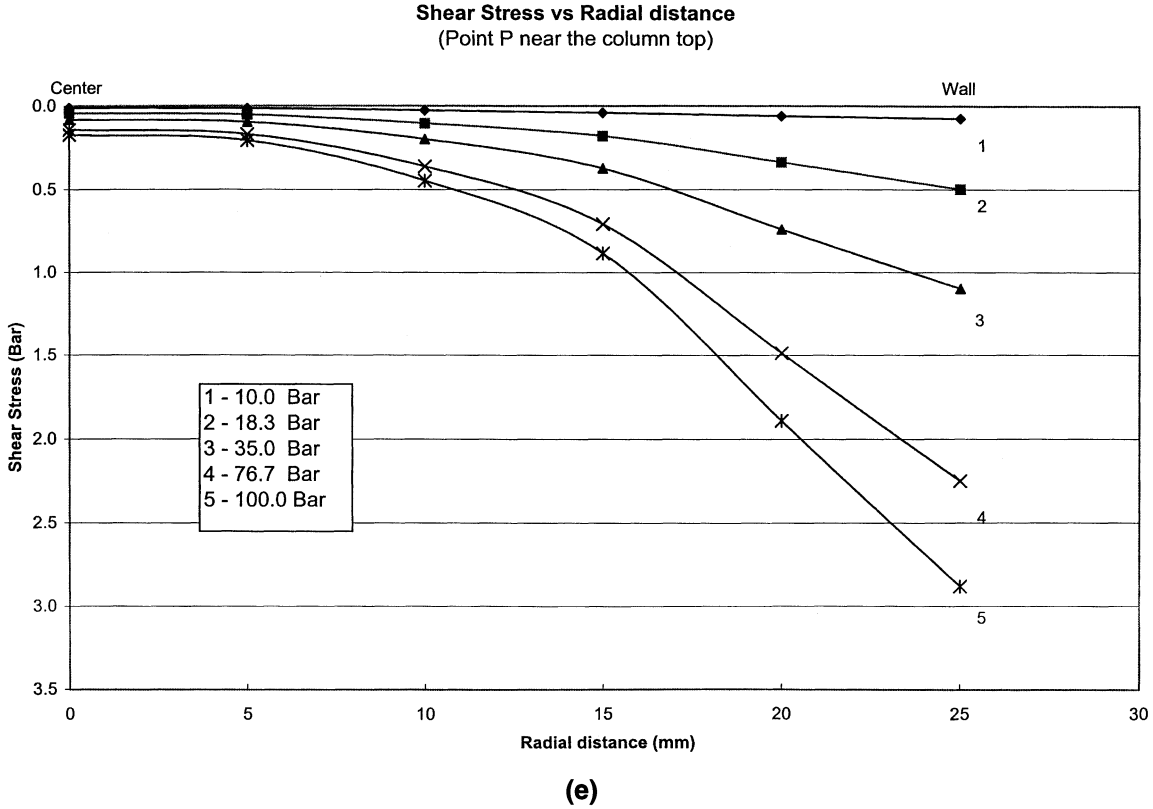


**Figure 13e. Distributions of the stress and strain (abscissa origin at the column axis or at the piston), at both ends of the bed and in its center.**

(e) radial distribution of the shear stress at $z = 150$ mm.

locity and the column efficiency reported by different authors (Farkas et al., 1997; Knox et al., 1976). The results illustrated in Figure 9 are also in good agreement with those published by Yun and Guiochon (1997) on the consolidation of chromatographic columns. This last set of results was obtained under experimental conditions very similar to those simulated in the present work.

A preliminary, independent result (Shalliker et al., 2003) confirms the modeling and calculation results presented in this work. Figure 15 shows the strain distribution inside a column that has been axially compressed under a 5.0 MPa stress. This distribution agrees qualitatively well with the calculated displacement distributions in Figures 10a and 10b. The material used was different because the refractive indices of the different brands of C18 silica that are available are spread in a wide enough range to preclude the use of most of them as packing material in the experiment described. Therefore, the frictional characteristics are different. Given the shape of the particles, it is probable that the internal angle of friction of the YMC packing material is intermediate between those of Kromasil and Zorbax (Guan et al., 1996). Furthermore, the glass column limits the magnitude of the stress that can be applied. However, the distribution of displacements is similar to the one calculated.

Obviously, these stress and strain distributions depend on several important experimental parameters. The most important are the internal and the interfacial coefficients of friction, correlated by the Potyondy (1961) relationship, the aspect ratio of the column and possibly its size, and the shape of the column head. Their influence will be studied in a forthcoming report (Ureta et al., 2003).

### *Influence of seepage under steady-state conditions*

To simulate steady-state flow through the packing material during the process of compressing and consolidating the slurry into a column bed, we assumed that the system was initially isotropic, homogeneous, and fully saturated. Automatic incrementation was used because, in a typical consolidation analysis, the increments can increase by several orders of magnitude during the simulation (Anon., 1998). Note that the liquid flows upward, arriving through the piston head, as in conventional operations with axial compression columns. Three points were chosen along the axis of the column: one against the piston ($R$, $z = 0$), one in the center of the column ($Q$, $z = 80$ mm), and one at one increment from the top of the bed ($P$, $z = 155$ mm); their locations are shown in Figure 10b.

The displacement and the pore pressure vs. time during the loading process are plotted in Figure 16. The displacements increase linearly over time as the piston pushes from the bottom of the column upward. As expected, the displacement is the largest at the bottom of the column ($R$) where the piston displacement is applied and it approaches 0.00 mm near the top of the column ($P$). The pore pressures were found to be zero over time at all positions inside the column

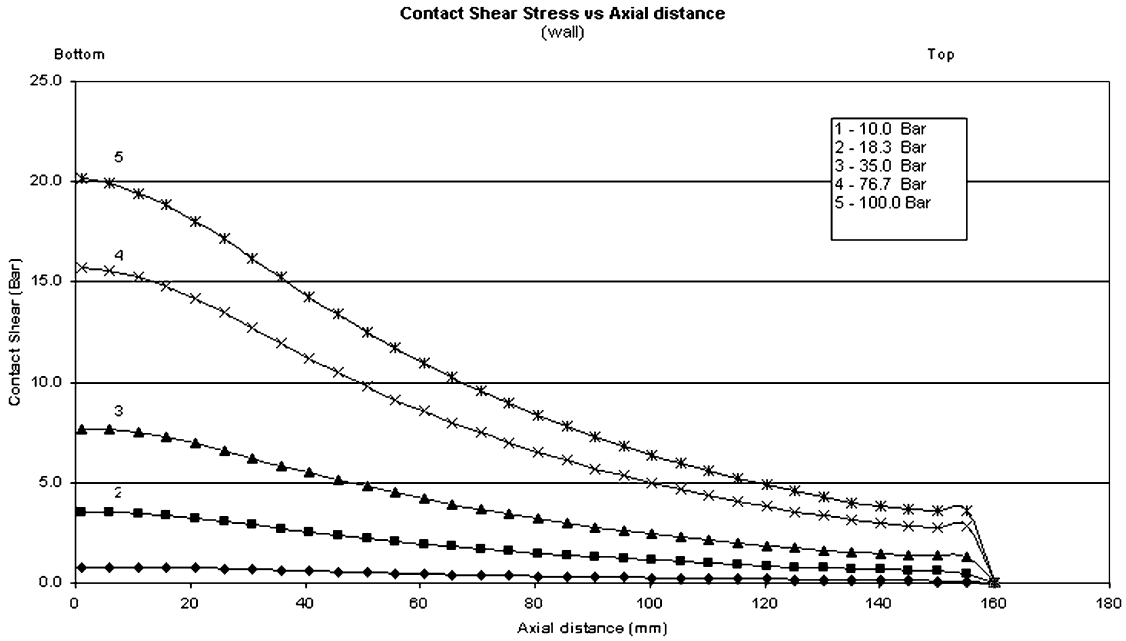


**Figure 14a,b. Axial distribution of the contact stress and strain (abscissa origin at the piston).**

(a) Contact shear (shear stress of the bed along the wall); (b) contact pressure (pressure of the bed against the wall).

during the whole packing process. This is consistent with the condition imposed in the steady-state analysis, that, at every time increment, the magnitude and the direction of the flow velocity are constant everywhere and, thus, must be equal to zero.

Calculations of the stress, displacement, and void fraction distributions in the bed gave results that were not significantly different from those of the calculations made without seepage and reported in the previous section. For this reason, no further investigations were carried out under steady-

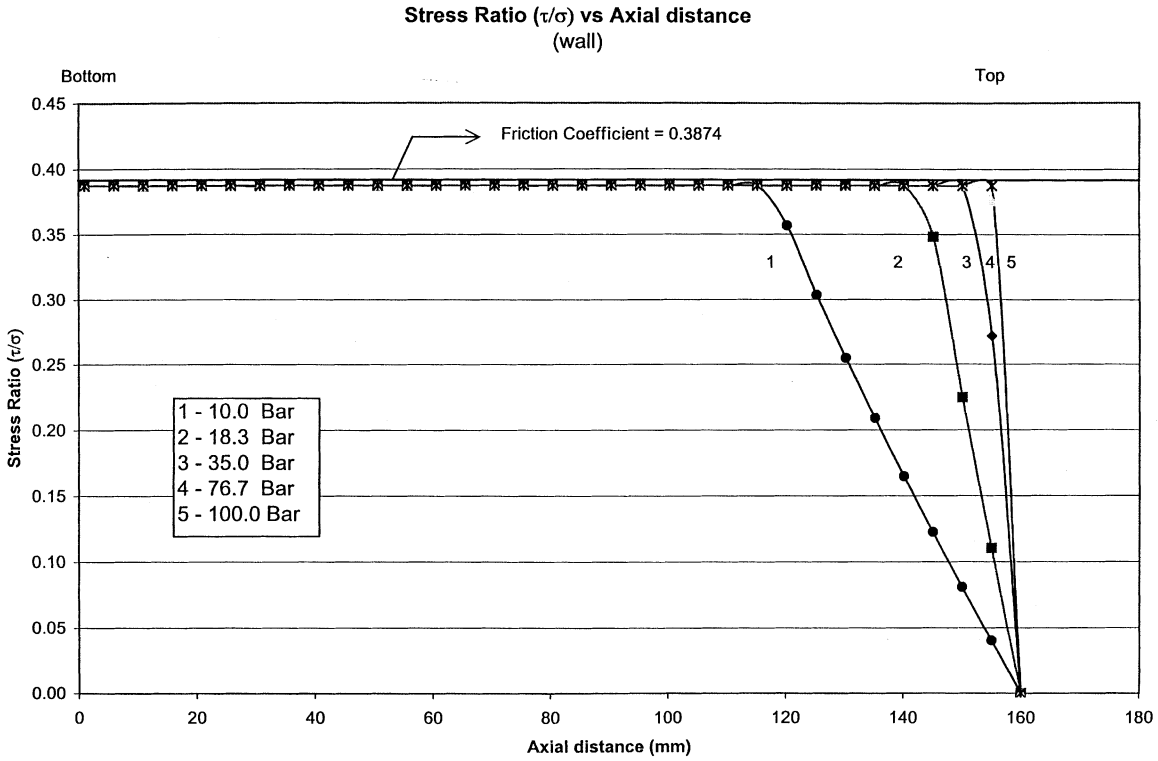


(c)

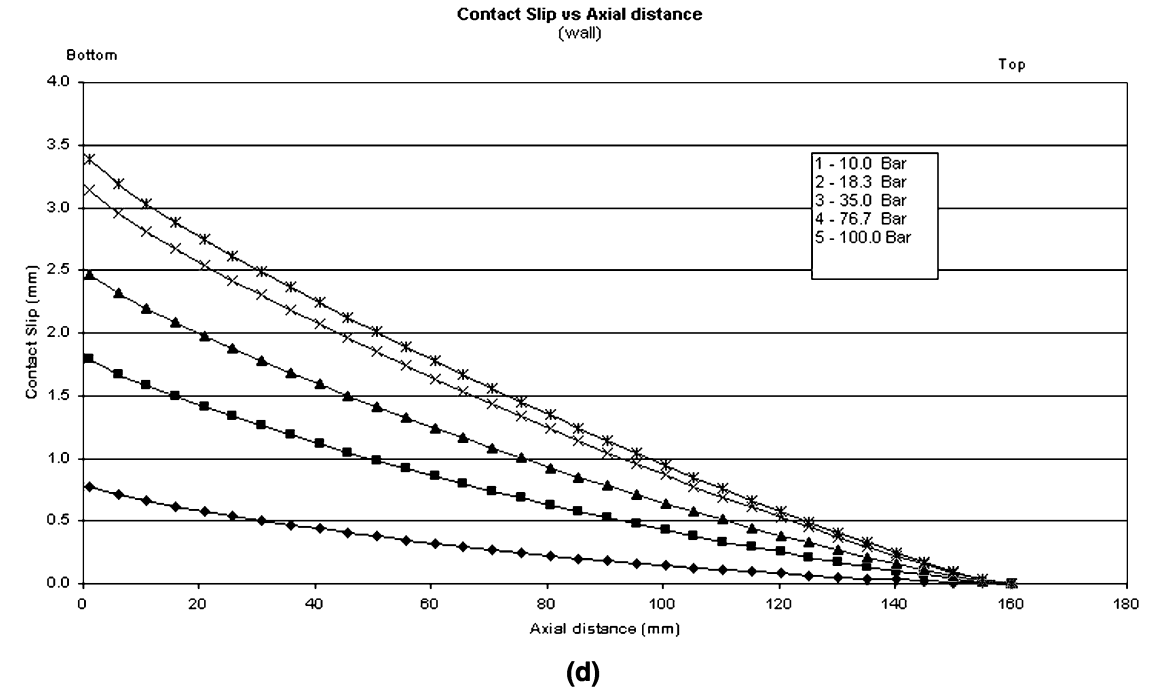


(d)

**Figure 14c,d. Axial distribution of the contact stress and strain (abscissa origin at the piston).**

(c) ratio of the contact shear and the contact pressure; (d) contact slip.

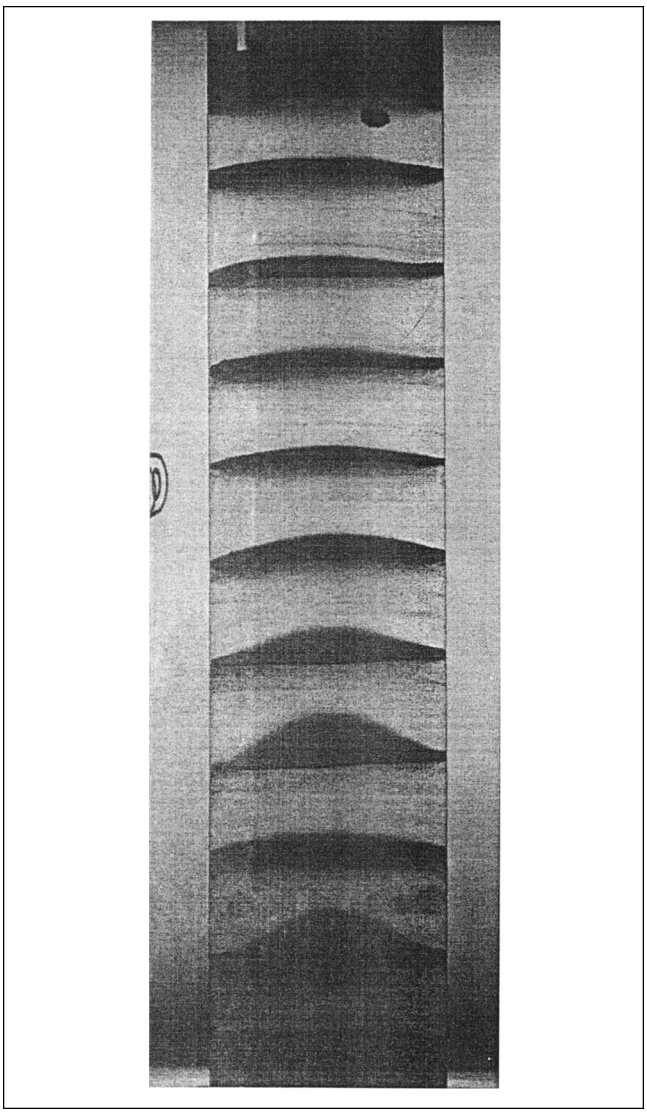

**Figure 15. Strain distribution in an axially compressed column (the piston moved upward, the axial stress applied was 5.0 MPa).**

Before consolidation, layers of a silica slurry (ca 1 cm thick) were interspersed with thin marker layers of a slurry of alumina particles. The mobile phase was carbon tetrachloride that has the same refractive index as the C18 silica used.

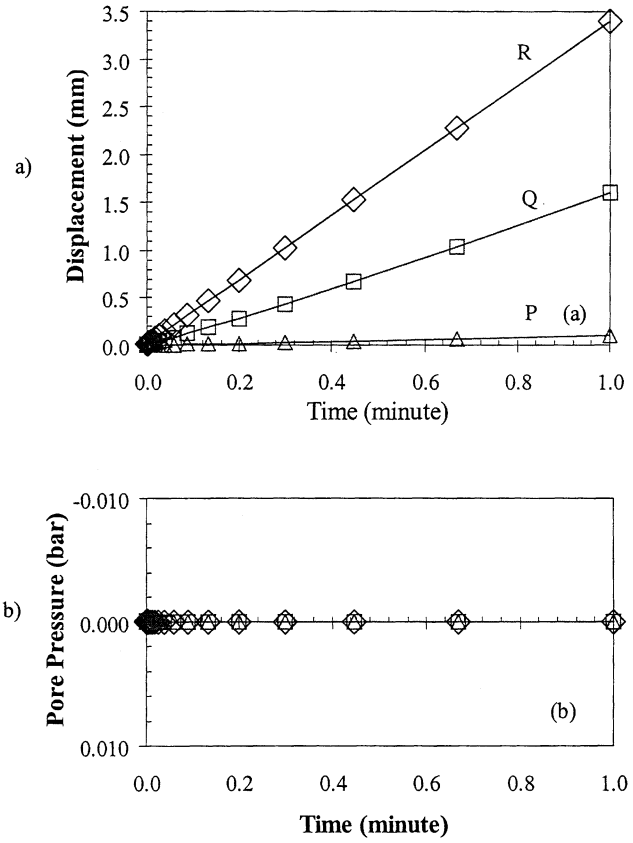


**Figure 16. Displacement of the bed along the wall and of the pore pressure during the packing process with seepage of the slurry solvent under steady-state conditions.**

(a) Displacement in points $P$ (top, $\Delta$), $Q$ (center, $\square$), and $R$ (bottom, $\diamond$); (b) pore pressure.

state conditions. Then, seepage under transient state conditions was assumed and investigated (see below).

### *Influence of seepage under transient conditions*

The rate at which the piston compresses the bed is a critical parameter in an investigation of the seepage effect under transient conditions. We carried out the calculations using a constant migration rate of the piston, corresponding to a displacement of 3.4 mm (axial compression of 10.0 MPa) in either one or two minutes. The piston was then held at its final displacement for two minutes in order to allow the computed pore pressure inside the column to dissipate. These loadings are typical of the actual packing process (Guiochon et al., 1999). The displacements calculated in points $P$, $Q$, and $R$ are reported in Figure 17a, for the two cases calculated. In both cases, the displacement was found to be maximum at the bottom of the column (Point $R$ where the displacement was applied and the rate was specified), to decrease along the column (away from the piston), and to approach zero at the top of the column (Figure 17a). Seepage does not influence the displacements under the experimental conditions used at a low migration rate of the piston (compression in 2 min). Note, however, that the displacement of point $Q$ is no longer linear at the faster rate (compression in 1 min).

As expected, the computed pore pressure increases as the piston pushes from the bottom during the packing process, as shown in Figure 17b. For the 2-min loading, once the piston stops pushing the bed upward, the pore pressures at the top of the column dissipate most rapidly since the solvent flows through the top of the column (flange, point $P$), as illustrated in Figure 17b. Since the drainage distances of Points $R$ and $Q$ are larger than at Point $P$, the pore pressure buildup at these points is greater but the drop in pressure when the piston stops is nearly instantaneous. With a displacement time of 2 min, the contour maps, the axial and radial distributions of the void fraction, stress and displacements obtained in the transient analysis (see Figures 18a and 18b) are closely simi-

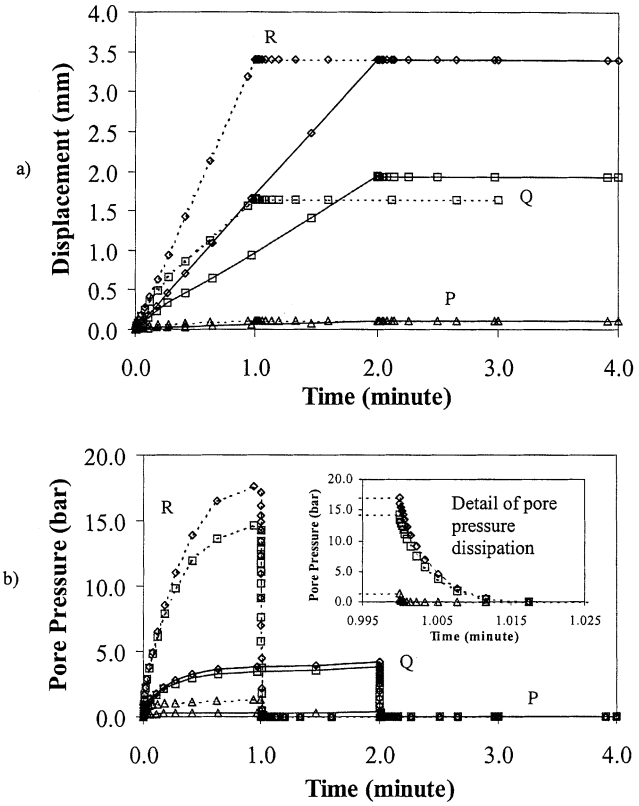


**Figure 17. Displacement of the bed along the wall and of the pore pressure during the packing process with seepage of the slurry solvent under transient conditions.**

Dotted line: loading of the stress from 0 to 10.0 MPa in 1 min; solid lines: same loading in 2 min. (a) Displacement in points *P* (top), *Q* (center), and *R* (bottom); (b) pore pressure.

lar to those obtained without accounting for the potential effect of seepage. This suggests that the pore pressures developed inside the HPLC columns during the 2 min loading process do not have any significant effect on the void ratio or the density of the beds of the packed columns.

The computed pore pressures at any point increase with increasing piston speed. The pore pressure increase everywhere is approximately 3.6 times greater during the 1 min than during the 2-min loading. Once the piston stops, the pore pressure dissipates rapidly (Figure 17b). The inset figure shows the pore pressure dissipation over a small time interval. Figures 18 and 19 compare the computed contour maps of the void ratio (Figure 18), and the mean compression stress (Figure 19) distributions at the end of the three packing processes, without seepage (a) and with transient seepage with compression taking place in 2(b) and 1(c) min. In this comparison, the uncoupled mechanical analysis can be considered to represent a column in which the piston is moved very slowly, so that no pore pressure builds up. Figures 18 and 19 show that, when the piston displacement is fast, the column obtained exhibits lesser degrees of axial and radial heterogeneity. The void ratio distribution is more uniform, especially at the bottom of the column, than for the column obtained at low compression rates. The stresses are also more

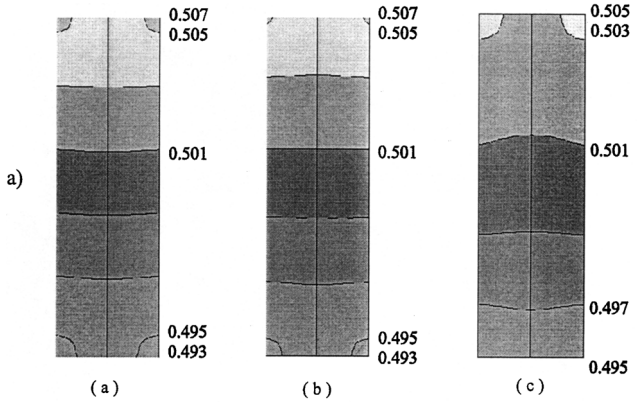


**Figure 18. Contour maps of distributions of the bed's void ratio obtained with compression under stress: (a) without seepage; (b) with seepage under transient conditions with a slow compression rate; and (c) with a fast compression rate.**

evenly distributed. Note that the third column bed (c) is more homogeneous than the second one (b), because the total ranges of variations of the void ratio (Figure 18) and of the stress (Figure 19) are smaller, the number of zones distinguished by the program is smaller and the remaining zones wider. A finer definition of the grids was not possible.

The numerical results of the model suggest that the rate of compression is important when packing HPLC columns. If the piston is pushed relatively fast (fast enough, given the compressibility and the permeability of the packing material, for the pore pressure to build up significantly), a more uniform column is produced than under static conditions. This result is consistent with laboratory observations, showing that a better column (presumably, the result of a less heterogeneous bed) is produced when the piston is pushed quickly (Godbille and Devaux, 1976).

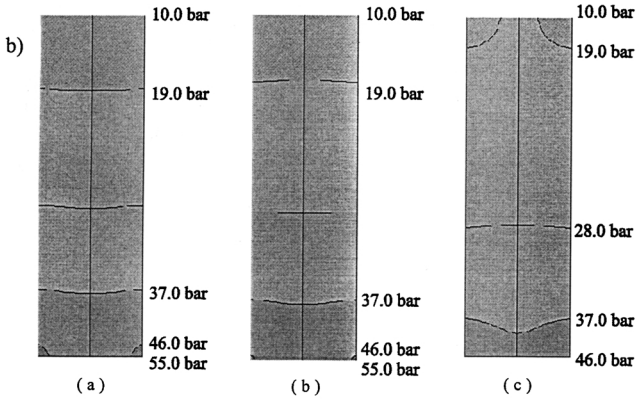


**Figure 19. Contour maps of distributions of the mean shear stress inside the beds obtained with compression under stress: (a) without seepage; (b) with seepage under transient conditions with a slow compression rate; and (c) with a fast compression rate.**

## Conclusion

The performance of a separation process based on preparative liquid chromatography depends strongly on the separation efficiency of the column used. Columns having a shorter HETP always give faster separations and larger production rates (Felinger and Guiochon, 1994). Accordingly, progress in the production of more efficient columns would markedly improve the economics of the process. We have shown that, during the preparation of the column, friction between the packing material and the wall of the column results in a nonuniform packing density, hence, nonuniform void ratio and permeability across the column cross-section. This radial heterogeneity of the bed causes a warping of the bands during their elution and significantly reduces the efficiency of the separation process. Unfortunately, rheology shows that the beds of chromatographic columns cannot be homogeneous since it is impossible to find a packing material with no friction coefficient against the wall. The preparation of the column beds should be carried out under such conditions that minimize the friction between the bed and the column wall.

The results obtained have shown the importance of seepage and of the rate of the piston movement during the compression and suggest the possibility of designing compression programs which could be realistic, yet give markedly more homogeneous packed beds, hence, more efficient columns. Other obvious applications of the model are the study of the influence of the friction angle of the packing material, and the use of nonplanar piston heads and end flange which, if properly profiled, could significantly reduce the degree of radial heterogeneity of the beds obtained by compression. These issues are currently under investigation and their conclusions will be reported later (Ureta et al., 2002).

## Notation

$a$ = cross-sectional area of the graduated burette
$A$ = cross-sectional area of the sample
$A_t$ = base area of the block used in tilt tests
$c$ = cohesion or cohesive strength of the material contact
$C_c$ = compression index
$C_s$ = swelling index
$C_v$ = coefficient of consolidation
$d$ = yield function intercept on the $q$ axis
$d_{10}$ = grain size corresponding to 10% finer
$d_{90}$ = grain size corresponding to 90% finer
$d_{\max}$ = maximum grain diameter
$d_{\min}$ = minimum grain diameter
$D$ = sample diameter
$e, e_v$ = void ratio of the packing material
$e_0$ = initial void ratio
$E$ = Young's modulus of the porous material
$f$ = coefficient of pore shape used in Carman-Kozeny formula
$F$ = linear Drucker-Prager yield surface function
$g$ = gravitational acceleration
$G_s$ = packing materials specific gravity
$h$ = hydraulic head
$h_f$ = elevation of methanol solvent in the standpipe above the discharge level at time $t$
$h_i$ = elevation of methanol solvent in the standpipe above the discharge level at time $t = 0$
$h_0$ = initial height
$h_t$ = height of plate
$H_0$ = initial height of the sample
$H_1$ = measured vertical distance using caliper
$H_2$ = depth of the shear box
$H_3$ = height of the top cap
$H_4$ = thickness of the filter paper
$J^{el}$ = logarithmic measure of the elastic volume change
$k$ = permeability coefficient or hydraulic conductivity
$K$ = intrinsic permeability
$K_g$ = bulk modulus of the solid grains
$K_i$ = the permeability of the porous medium in the $i$ direction, where $i = x, y, z$
$L$ = length of the sample
$L_t$ = length of the plate used in tilt tests
$m$ = mobile phase
$M_d$ = mass of the dry sample
$M_e$ = external mass occupied by solvent around the particles
$M_i$ = internal mass occupied by solvent inside the particles
$M_T$ = total mass of the packed bed
$M_u$ = inaccessible mass occupied by the solids of the silica particles
$n$ = number of elements
$n$ = porosity of the porous medium
$N$ = normal load
$p$ = mean stress
$p_0$ = initial value of the equivalent pressure or stress
$p_t^{el}$ = elastic tensile strength of the material
$q$ = Mises equivalent stress
$R$ = resisting force against sliding
$s$ = stationary phase
$S$ = specific surface area
$S_s$ = specified storage where the volume of fluid released from a unit volume of saturated porous medium for a unit decline in hydraulic head, $h$
$t$ = time
$T$ = shear force
$U$ = degree of consolidation
$U_z$ = axial displacement
UTOL = maximum pore pressure that was allowed to dissipate in each time increment
$v_x$, $v_y$, and $v_z$ = the specific discharge (volume flow rate of permeating liquid per unit area) in the $x$, $y$ and $z$ direction, respectively
$v_w$ = the magnitude of the velocity of the pore fluid in Forchheimer's flow law
$V$ = present volume
$V_1$ = initial volume
$V_e$ = external pores volume
$V_i$ = internal pores volume
$V_0$ = total volume occupied by solvent
$V_{\text{particles}}$ = volume of silica particles, occupied by the volume inaccessible to the solvent and the internal pores volume
$V_s$ = total volume of silica particles
$V_T$ = total column volume
$V_{u^*}$ = volume inaccessible to the solvent
$W$ = weight of phenolic block

### *Greek letters*

$\alpha$ = angle between a plane surface to the horizontal surface
$\alpha_{pm}$ = compressibility of the porous medium
$\beta_F$ = the velocity coefficient in Forchheimer's flow law
$\beta$ = slope of the yield function in the $p$-$q$ stress space
$\beta_F$ = the velocity coefficient in Forchheimer's flow law
$\beta_w$ = compressibility of the permeating fluid
$\Delta h$ = vertical deformation due to axially applied load
$\Delta l$ = typical element dimension
$\Delta t$ = time increment used in ABAQUS (1998)
$\delta$ = interface friction angle
$\epsilon_e$ = external porosity
$\epsilon_i$ = internal porosity
$\epsilon_T$ = total porosity
$\epsilon_v$ = volumetric strain
$\epsilon_z$ = axial strain
$Y_w$ = specific weight of the wetting liquid or solvent
$\phi$ = internal friction angle
$\phi_p$ = peak friction angle

$\phi_r$ = residual friction angle
$\kappa$ = logarithmic bulk modulus for porous elastic model
$\mu$ = dynamic viscosity of the fluid
$\rho_{d0}$ = initial dry density
$r_{\text{dry}}$ = dry or apparent density of packed bed
$\rho_{\text{particles}}$ = density of silica particles
$r_u$ = density of silica solids
$\rho_w, \rho$ = density of the solvent or fluid
$\sigma$ = total or axially applied stress (normal stress)
$\sigma_{11}, \sigma_{22}, \sigma_{33}$ = principle stresses
$\sigma_y$ = normal stress
$\sigma'$ = effective stress
$\sigma'_P$ = preconsolidation pressure
$T, T_{xy}$ = shear stress
$\psi$ = dilation angle

## Acknowledgments

This work was supported in part by Grant DE-FG05-88-ER13869 of the U.S. Department of Energy and by the cooperative agreement between the University of Tennessee and the Oak Ridge National Laboratory.

## Literature Cited

Anon., *ABAQUS/Standard User's Manual,* Habbitt, Karlsson and Sorensen, RI, version 5.8 (1998).
Baker, A. J., and D. W. Pepper, *Finite Elements 1-2-3,* McGraw-Hill, New York (1991).
Bird, R. B., W. E. Stewart, and E. N. Lightfoot, *Transport Phenomena*, Wiley, New York (1960).
Broyles, B. S., R. A. Shalliker, D. E. Cherrak, and G. Guiochon, "Visualization of Viscous Fingering in Chromatographic Columns," *J. Chromatog. A*, **822**, 173 (1998).
Broyles, B. S., R. A. Shalliker, and G. Guiochon, "Visualization of Sample Introduction in Liquid Chromatography Columns. The Influence of the Frit Diameter," *J. Chromatog. A*, **855**, 367 (1999a).
Broyles, B. S., R. A. Shalliker, and G. Guiochon, "Visualization of Sample Introduction in Liquid Chromatography Columns: Contribution of a Flow Distributor on the Sample Band Shape," *J. Chromatog. A*, **865**, 83 (1999b).
Carman, P. C., *Flow of Gases through Porous Media*, Academic Press, New York (1956).
Cherrak, D. E., and G. Guiochon, "Phenomenological Study of The Bed/Wall Friction in Axially Compressed Packed Chromatographic Columns," *J. Chromatog. A*, **911**, 147 (2001).
Cook, R. D., *Finite Element Modeling for Stress Analysis*, Wiley, New York (1995).
Desai, C. S., and H. J. Siriwardane, *Constitutive Laws for Engineering Materials with Emphasis on Geologic Materials*, Prentice-Hall, Englewood Cliffs, NJ (1984).
Drucker, D. C., and W. Prager, "Soil Mechanics and Plastic Analysis or Limit Design," *Quart. Appl. Math.*, **10**, 157 (1952).
Farkas, T., M. J. Sepaniak, and G. Guiochon, "Radial Distribution of the Flow Velocity, The Column Efficiency, and the Concentration Profile at the Outlet of a Preparative Scale HPLC Column," *AIChE J.*, **43**, 1964 (1997).
Felinger, A., and G. Guiochon, "Optimizing Experimental Conditions for Minimum Production Cost in Preparative Chromatography," *AIChE J.*, **40**, 594 (1994).
Freeze, R. A., and J. A. Cherry, *Groundwater*, Prentice-Hall, Englewood Cliffs, NJ (1979).
Godbille, E., and P. Devaux, "Use of an 18-mm I.D. Column for Analytical- and Preparative-scale High-Pressure Liquid Chromatography," *J. Chromatog.*, **122**, 317 (1976).
Guan, H., G. Guiochon, D. Coffey, E. Davis, K. Gulakowski, and D. W. Smith, "Study of the Physico-chemical Properties Of Some Packing Materials: II. General Properties of the Particles," *J. Chromatog. A*, **736**, 21 (1996).
Guiochon, G., D. Drumm, and D. E. Cherrak, "Evidence of a Wall Friction Effect in the Consolidation of Beds of Packing Materials in Chromatographic Columns," *J. Chromatog. A*, **835**, 41 (1999).
Guiochon, G., T. Farkas, H. Guan-Sajonz, J.-H. Koh, M. Sarker, B. J. Stanley, and T. Yun, "Consolidation of Particles Beds and Packing of Chromatographic Columns," *J. Chromatog. A*, **762**, 83 (1997).
Guiochon, G., and M. Sarker, "Consolidation of the Packing Material in Chromatographic Columns under Dynamic Axial Compression: I. Fundamental Study," *J. Chromatog. A*, **704**, 247 (1995).
Huber, J. F. K., J. C. Kraak, and H. Veening, "Rapid Separation of Metal Chelates by Column Liquid-Liquid Chromatography Using Ultraviolet Detection," *Anal. Chem.*, **44**, 1554 (1972).
Knox, J. H., G. R. Laird, and P. A. Raven, "Interaction of Axial and Radial Dispersion in Liquid Chromatography in Relation to the 'Infinite diameter Effect'," *J. Chromatog.*, **122**, 129 (1976).
Lambe, T. W., and R. B. Whitman, *Soil Mechanics. SI Version*, Wiley, New York (1979).
Mihlbachler, K., T. Kollmann, A. Seidel-Morgenstern, J. Tomas, and G. Guiochon, "Measurement of the Degree of Cohesion of Two Native Silica Packing Materials," *J. Chromatog. A*, **818**, 155 (1998).
Poole, C. F., and S. K. Poole, *Chromatography Today*, 2nd ed., Elsevier, Amsterdam (1993).
Popov, E. P., *Introduction to Mechanics of Solids*, Prentice-Hall, Englewood Cliff, NJ (1968).
Potyondy, J. G., "Skin Friction between Various Soils and Construction Materials," *Geotechnique*, **11**, 339 (1961).
Roussel-Uclaf, Romainville, France, "Chromatographic Device," U.S. Patent No. 3,966,609 (June 17, 1976).
Sarker, M., A. M. Katti, and G. Guiochon, "Consolidation of the Packing Material in Chromatographic Columns under Dynamic Axial Compression: II. Consolidation and Breakage of Several Packing Materials," *J. Chromatog. A*, **719**, 275 (1996).
Shalliker, R. A., B. S. Broyles, and G. Guiochon, "On-column Visualization of Sample Migration in Liquid Chromatography," *Anal. Chem.*, **72**, 323 (2000a).
Shalliker, R. A., B. S. Broyles, and G. Guiochon, "Physical Evidence of Two Wall Effects in Liquid Chromatography," *J. Chromatog. A*, **888**, 1 (2000b).
Shalliker, R. A., V. Wong, B. S. Broyles, and G. Guiochon, "Visualization of Bed Compression in an Axial Compression Liquid Chromatography Column," *J. Chromatog. A*, **977**, 213 (2002).
Snyder, L. R., and J. J. Kirkland, *Introduction to Modern Liquid Chromatography*, 2nd ed., New York, Wiley (1979).
Tallarek, U., K. Albert, E. Bayer, and G. Guiochon, "Measurement of the Transverse and Axial Apparent Dispersion Coefficients in a Packed Bed by Pulsed Field Gradient Nuclear Magnetic Resonance," *AIChE J.*, **42**, 3041 (1996).
Train, D., "An Investigation into the Compaction of Powders," *J. Pharm. Pharmac.*, **8**, 745 (1956).
Train, D., "Transmission of Forces through a Powder Mass during the Process of Pelleting," *Trans. Instn. Chem. Engrs.*, **35**, 258 (1957).
Ureta, J., E. Drumm, and G. Guiochon, "Application of The Rheology of Particulate Materials to The Study of The Properties of Column Beds: III. Influence of Experimental Parameters," in press (2003).
Verzele, M., and C. Dewaele, *Preparative High Performance Liquid Chromatography*, TEC, Ghent, Belgium (1986).
Yew, B. G., "Application of Soil Mechanics and the Finite Element Method to High Performance Liquid Chromatography Columns," MS Thesis Diss., The University of Tennessee, Knoxville, TN (2000).
Yew, B. G., E. Drumm, and G. Guiochon, "Application of The Rheology of Particulate Materials to the Study of the Properties of Column Beds: I. Acquisition of The Relevant Parameters," AIChE J., **49** (2003) (Companion paper).
Yuan, Q. S., A. Rosenfeld, T. W. Root, D. J. Klingenberg, and E. N. Lightfoot, "Flow Distribution in Chromatographic Columns," *J. Chromatog. A*, **831**, 149 (1998).
Yun, T., and G. Guiochon, "Visualization of the Heterogeneity of a Column Bed," *J. Chromatog. A*, **760**, 17 (1997).

*Manuscript received Oct. 26, 2001, and revision received Aug. 27, 2002.*